

A two-component model of hadron production applied to p_t spectra from 5 TeV and 13 TeV p - p collisions at the large hadron collider

Thomas A. Trainor

CENPA 354290, University of Washington, Seattle, Washington 98195

(Dated: April 26, 2021)

The ALICE collaboration at the large hadron collider (LHC) recently reported high-statistics p_t spectrum data from 5 TeV and 13 TeV p - p collisions. Particle data for each energy were partitioned into event classes based on the total yields within two disjoint pseudorapidity η intervals denoted by acronyms V0M and SPD. For each energy the spectra resulting from the two selection methods were then compared to a minimum-bias INEL > 0 average over the entire event population. The nominal goal was determination of the role of jets in high-multiplicity p - p collisions and especially the jet contribution to the low- p_t parts of spectra. A related motivation was response to recent claims of “collective” behavior and other nominal indicators of quark-gluon plasma (QGP) formation in small collision systems. In the present study a two-component (soft + hard) model (TCM) of hadron production in p - p collisions is applied to the ALICE spectrum data. As in previous TCM studies of a variety of A-B collision systems the jet and nonjet contributions to p - p spectra are accurately separated over the entire p_t acceptance. Distinction is maintained among spectrum normalizations, jet contributions to spectra and systematic biases resulting from V0M and SPD event selection. The statistical significance of data-model differences is established. The effect of *sphericity* (azimuthal asymmetry measure nominally sensitive to jet production) on ensemble-mean p_t vs event multiplicity n_{ch} is investigated and found to have little relation to jet production. The general results of the TCM analysis are as expected from a conventional QCD description of jet production in p - p collisions.

PACS numbers: 12.38.Qk, 13.87.Fh, 25.75.Ag, 25.75.Bh, 25.75.Ld, 25.75.Nq

I. INTRODUCTION

Claims of quark-gluon plasma (QGP) formation in Au-Au collisions at the relativistic heavy ion collider (RHIC) and subsequently in Pb-Pb collisions at the large hadron collider (LHC) were based on certain data features initially seen as unique to more-central A-A collisions and not appearing in small asymmetric A-B control systems such as d -Au or p -Pb where QCD theory suggested that QGP formation should be unlikely. However, in recent years similar features have been observed in LHC data for p -Pb collisions and high-charge-multiplicity p - p collisions and have been interpreted as evidence for QGP formation in small collision systems [1, 2]. But the recent LHC results could also be interpreted to indicate that data features conventionally associated with QGP formation may result from unexceptional QCD processes.

The ALICE collaboration recently published a comprehensive high-statistics study of p_t spectra from 5 TeV and 13 TeV p - p collisions [3]. The analysis employs two methods to sort collision events into ten multiplicity classes each and application of *sphericity* S_0 , a measure of the azimuthal nonuniformity of distributed $\vec{p}_t(\phi)$, to estimate the “jettiness” of events. Several methods are applied to determine variation of spectrum shape with charge multiplicity, event-selection method and sphericity.

The study reported in Ref. [3] is motivated in part by claimed observation in p - p and p -Pb collisions of evidence for radial and elliptic flow (“collectivity”) [4, 5] as well as strangeness enhancement [6] similar to that observed in more-central A-A collisions and attributed there to QGP formation. Observation of such effects in low-density sys-

tems occupying small space-time volumes runs counter to initial theoretical expectations concerning QGP formation. The study seeks to understand hadron production associated with jets in relation to soft particle production: “The aim of this study is to investigate the importance of jets in high-multiplicity pp collisions and their contribution to charged-particle production at low p_T .”

The phenomenology of high-energy p - p collision data serves as an essential reference for high-energy p -A and A-A collisions, specifically regarding claims of novel physical mechanisms such as QGP formation [7] or possible manifestations of hydrodynamic flows even in small collision systems [8, 9]. One can formulate a set of critical questions addressed to available p - p data: (a) What is the evidence for or against azimuthally symmetric radial flow, and for or against elliptic flow and “higher harmonics” as manifestations of azimuthal asymmetry? (b) Are nominally flow-related azimuthal features certainly disjoint from jet production? (c) Are jet contributions to spectra significantly modified by a dense medium (i.e. QGP)? (d) Does the charge-multiplicity (n_{ch}) dependence of certain data features reflect the onset of such a medium with increasing particle density? If the QGP scenario is valid then systematic behavior of various data features should be synchronized with emergence of a *common* underlying dense medium. Are comprehensive data trends consistent with such expected synchronization?

A two-component (soft + hard) model (TCM) of hadron production near mid-rapidity in A-B collisions was initially derived from the charge-multiplicity n_{ch} dependence of p_t spectra from 200 GeV p - p collisions [10]. The n_{ch} dependence of yields, spectra and two-particle correlations has played a key role in establishing (a) the

nature of hadron production mechanisms in p - p collisions and (b) that the TCM hard component of p_t spectra is *quantitatively* consistent with predictions based on event-wise reconstructed jets [11–13]. The question of recently-claimed collectivity or flows in small (p - p and p - A) systems has been addressed in terms of the resolved TCM soft and hard components and evidence (or not) for radial flow in differential studies of p_t spectra [14–16].

Reference [17] reported previous TCM analysis of 13 TeV p - p spectra that serves as a precursor to the present study (see App. A). Then-available spectrum data [18] were presented only as ratios to minimum-bias spectra and only for a limited n_{ch} range. The present study extends those results utilizing both 5 TeV and 13 TeV data. Spectra for the two energies and for two methods of event selection, V0M and SPD, are decomposed into soft and hard components for ten event multiplicity classes each. Spectrum biases resulting from event selection methods are evaluated and compared. The quality of the TCM description is determined via data-model *differences* (not ratios) compared to statistical uncertainties (Z -scores) as a significance test. A TCM for ensemble-mean p_t or \bar{p}_t is defined and applied to \bar{p}_t vs n_{ch} data from Ref. [3]. Evolution of the $\bar{p}_t(n_{ch})$ trend with sphericity S_0 is examined in detail – especially the relation of S_0 to dijet production. An ironic result emerges.

The TCM serves as an accurate reference for A-B collision systems that is not derived from fits to individual spectra. The TCM is required to describe diverse data formats applied to a broad array of collision systems self-consistently. It precisely separates jet and nonjet data contributions, greatly facilitating and simplifying data interpretation. Data-TCM deviations may reveal systematic data biases as in the present study or identify new physics beyond conventional models as in Ref. [14].

This article is arranged as follows: Section II summarizes p - p spectrum data, methods and conclusions reported in Ref. [3]. Section III describes the TCM for p - p p_t spectra. Section IV summarizes selection biases resulting from two event-selection criteria and their evolution with event multiplicity n_{ch} . Section V reviews some p_t spectrum shape measures. Section VI describes the TCM for ensemble \bar{p}_t and reviews results from Ref. [3] for evolution of $\bar{p}_t(n_{ch})$ trends with varying sphericity S_0 . Section VII discusses systematic uncertainties. Sections VIII and IX present discussion and summary.

II. 5 AND 13 TeV p - p p_t SPECTRUM DATA

Reference [3] reports p_t spectra from 5 and 13 TeV p - p collisions for two event selection methods (V0M and SPD) and for ten charge-multiplicity classes each. For each energy the same minimum-bias (INEL > 0) event ensemble is effectively sorted into multiplicity classes in two ways. The p_t acceptance is $p_t \in [0.15, 20]$ GeV/c. The angular acceptance is 2π on azimuth and $|\eta| \leq 0.8$ on pseudorapidity. The total event numbers are 105 and

60 million for 5 and 13 TeV respectively. The basic p_t spectra are further analyzed via several methods. As noted, the stated main goal of the study is to understand the role of jets in high-multiplicity p - p collisions.

A. Motivation and strategy

The context presented for the spectrum analysis reported in Ref. [3] is claimed observation at the LHC of collectivity – i.e. radial [4, 19] and anisotropic (e.g. elliptic, higher harmonic) [5] flows – and strangeness enhancement [6] in p - p and p -Pb collisions whereas those phenomena had been designated as indicators of QGP formation only in high-density A - A collision systems. A variety of models based on hydrodynamics, string percolation, multiparton interactions or fragmentation of saturated gluon states are “...able to describe...qualitatively well...some features of data.” However, concerns have been expressed about interpretations of data from small collision systems in terms of QGP formation without a more-rigorous examination of data and models [20].

It is asserted that a p_t spectrum “carries information of the dynamics of soft and hard interactions.” Reference is made to three p_t intervals: $p_t > 10$ GeV/c is said to be “quantitatively well described by perturbative QCD (pQCD) calculations.”¹ Below that limit one must “resort to phenomenological QCD inspired models [i.e. Monte Carlo models].” Novel effects claimed for p - p and p -Pb collisions are said to appear in $p_t < 2$ GeV/c and $p_t \in [2, 10]$ GeV/c. Reference [3] asserts that “The present paper reports a novel multi-differential analysis aimed at understanding charged-particle production associated to partonic scatterings with large momentum transfer and their possible correlations with soft particle production.” In essence, Ref. [3] poses the question: what is the jet contribution to hadron spectra at low p_t ?

B. p - p p_t spectrum data

Figures 1 and 2 show spectra (points) for 5 TeV and 13 TeV respectively. Panels (a) and (c) show spectra for sorting criteria V0M and SPD respectively multiplied by successive powers of ten from lowest to highest multiplicity in a conventional log-log plot format. The solid curves represent the TCM described in Sec. III. The TCM is not derived from fits to individual spectra. Panels (b) and (d) show data/model ratios based on the TCM. Line types for the four highest- n_{ch} classes vary as solid, dashed, dotted and dash-dotted. That convention is applied consistently in what follows unless explicitly noted. In those ratios certain “noise” components appear as common to

¹ A pQCD (i.e. jet) description is quantitatively consistent with the p - p p_t spectrum *hard component* down to 0.5 GeV/c [11].

multiple spectra. It is possible that those features arise from efficiency corrections generated by a Monte Carlo simulation with a more-limited number of events. Power-law fits to spectra above 6 GeV/c are used to infer a power-law exponent n which is observed to decrease in magnitude with increasing n_{ch} (but see Sec. V A). Note that spectra as plotted in Ref. [3] and Figs. 1 and 2 (a,c) below are in the form $d^2n_{ch}/dp_t d\eta$ whereas $\bar{\rho}_0(p_t; n_{ch})$ corresponding to $\bar{\rho}_0(y_t; n_{ch})$ as defined in Eq. (1) includes an additional factor p_t in its denominator.

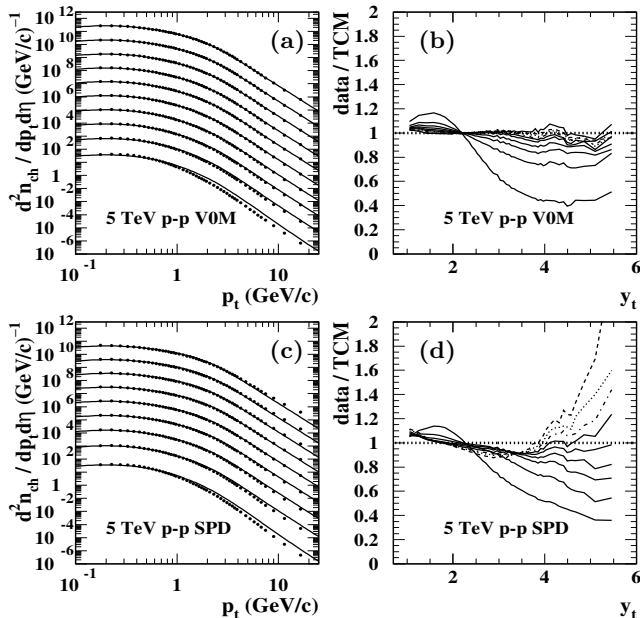


FIG. 1: Left: p_t spectra from ten (V0M) or nine (SPD) multiplicity classes of 5 TeV p - p collisions for V0M (a) and SPD (c) event selection. Right: data/TCM spectrum ratios for data in the left panels for V0M (b) and SPD (d) event selection.

C. Ensemble-mean \bar{p}_t vs n_{ch} and sphericity

Spectra are also sorted according to sphericity $S_0 \in [0, 1]$ or $S_0(\%) \in [0\%, 100\%]$ [see Eq. (14)], said to be a measure of the “jettiness” of the event-wise $\vec{p}_t(\phi)$ azimuth distribution, where $S_0 \approx 1$ or 100% is associated with near-isotropic events. For ten classes of sphericity S_0 ensemble-mean \bar{p}_t vs multiplicity n_{ch} trends for 13 TeV data are evaluated. Event multiplicity classes are defined within $|\eta| < 0.8$ (i.e. SPD selection). Reference [3] states: “Since the goal of the present study is to separate jet events from isotropic ones, we study different sphericity classes for a given multiplicity value.” “...the most jet-like and [most] isotropic events will be referred to as 0-10% and 90-100% sphericity classes, respectively.”

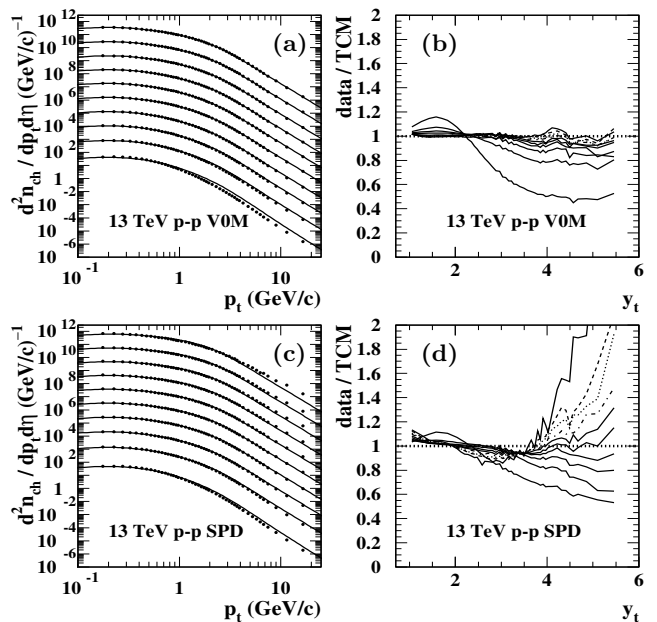


FIG. 2: Left: p_t spectra from ten multiplicity classes of 13 TeV p - p collisions for V0M (a) and SPD (c) event selection. Right: data/TCM spectrum ratios for data in the left panels for V0M (b) and SPD (d) event selection.

D. Summary and conclusions

The abstract of Ref. [3] asserts that p_t spectra exhibit little energy dependence (between 5 and 13 TeV), and the high- p_t tails of spectra increase faster than linearly with event multiplicity n_{ch} . Regarding the sphericity study “For low- (high-) sphericity events, corresponding to jet-like (isotropic) events, the average p_T is higher (smaller) than that measured in INEL > 0 pp collisions.”

Although it is reported that ensemble-mean \bar{p}_t increases with decreasing sphericity (expected to indicate increased jettiness) the observed *shape* of \bar{p}_t vs n_{ch} doesn’t change significantly with sphericity (contradicting the expectation, see Sec. VI C). Sphericity results are said to “illustrate the difficulties for the [Monte Carlo] models to describe different observables once they are differentially analyzed as a function of several variables.”

The summary states that “For a fixed center-of-mass energy, particle production above $p_T = 0.5$ GeV/c exhibits a remarkable multiplicity dependence. Namely, for transverse momenta below 0.5 GeV/c, the ratio of the multiplicity dependent spectra to those for INEL > 0 pp collisions is rather constant, and for higher momenta, it shows a significant p_t dependence. The behavior observed for each of the two multiplicity estimators are consistent within the $\langle dN_{ch}/d\eta \rangle$ interval defined by the V0M multiplicity estimator, which gives a $\langle dN_{ch}/d\eta \rangle$ reach of ~ 25 . For the highest V0M multiplicity class, the ratio increases going from $p_T = 0.5$ GeV/c up to $p_T \approx 4$ GeV/c, then for higher p_T , it shows a smaller increase.” Those qualitative observations contrast with highly dif-

ferential and quantitative TCM results from the present study as presented below in Secs. III - VI.

III. p-p p_t SPECTRUM TCM

The p_t spectrum TCM, first reported for 200 GeV p - p collisions in Ref. [10], is basically consistent with the TCM first reported in Ref. [21] in response to UA1 “mini-jets” from the CERN $Spp\bar{p}S$. The TCM provides an accurate description of yields, spectra and two-particle correlations for A-B collision systems based on linear superposition of N - N or parton-parton collisions. In general, the TCM serves as a *predictive reference* for any collision system. Deviations from the TCM then provide systematic and quantitative information on details of collision mechanisms. In this section the spectrum TCM is reviewed and then applied to 5 TeV and 13 TeV p_t spectra for two event selection methods from Ref. [3].

A. p_t spectrum TCM for unidentified hadrons

The p_t or y_t spectrum TCM is by definition the sum of soft and hard components with details inferred from data (e.g. Ref. [10]). For p - p collisions

$$\begin{aligned} \bar{\rho}_0(y_t; n_{ch}) &\approx \frac{d^2 n_{ch}}{y_t dy_t d\eta} \\ &\approx \bar{\rho}_s(n_{ch}) \hat{S}_0(y_t) + \bar{\rho}_h(n_{ch}) \hat{H}_0(y_t), \end{aligned} \quad (1)$$

where n_{ch} is an event-class index and factorization of the dependences on y_t and n_{ch} is a central feature of the spectrum TCM inferred from 200 GeV p - p spectrum data in Ref. [10]. The motivation for transverse rapidity $y_{ti} \equiv \ln[(p_t + m_{ti})/m_i]$ (applied to hadron species i) is explained in Sec. IIIB. The y_t integral of Eq. (1) is $\bar{\rho}_0 \equiv n_{ch}/\Delta\eta = \bar{\rho}_s + \bar{\rho}_h$, a sum of soft and hard charge densities. $\hat{S}_0(y_t)$ and $\hat{H}_0(y_t)$ are unit-normal model functions independent of n_{ch} . The centrally-important relation $\bar{\rho}_h \approx \alpha \bar{\rho}_s^2$ with $\alpha = O(0.01)$ is inferred from p - p spectrum data [10, 14, 17]. $\bar{\rho}_s$ is then obtained from measured $\bar{\rho}_0$ as the root of the quadratic equation $\bar{\rho}_0 = \bar{\rho}_s + \alpha \bar{\rho}_s^2$ with α determined by an energy trend derived from p - p spectrum data covering a large energy interval [17]. It is important to distinguish TCM model elements from spectrum data soft and hard components. It is useful to recall that y_t values 1, 2, 3, 4 and 5 are approximately equivalent to p_t values 0.15, 0.5, 1.4, 3.8 and 10 GeV/ c .

B. p_t spectrum TCM model functions

The p - p p_t spectrum soft component is most efficiently described on transverse mass m_t whereas the spectrum hard component is most efficiently described on transverse rapidity y_t . The spectrum TCM thus requires a heterogeneous set of variables for its simplest definition.

The components can be easily transformed from one variable to the other by Jacobian factors defined below.

Given spectrum data in the form of Eq. (1) the unit-normal spectrum soft-component model $\hat{S}_0(y_t)$ is defined as the asymptotic limit of data spectra normalized in the form $X(y_t) \equiv \bar{\rho}_0(y_t; n_{ch})/\bar{\rho}_s$ as n_{ch} goes to zero. Hard components of data spectra are then defined as complementary to soft components, with the explicit form

$$Y(y_t) \equiv \frac{1}{\alpha \bar{\rho}_s} \left[X(y_t) - \hat{S}_0(y_t) \right], \quad (2)$$

directly comparable with TCM model function $\hat{H}_0(y_t)$.

The data soft component for a specific hadron species i is typically well described by a Lévy distribution on $m_{ti} = \sqrt{p_t^2 + m_i^2}$. The unit-integral soft-component model is

$$\hat{S}_{0i}(m_{ti}) = \frac{A_i}{[1 + (m_{ti} - m_i)/n_i T_i]^{n_i}}, \quad (3)$$

where m_{ti} is the transverse mass-energy for hadron species i with mass m_i , n_i is the Lévy exponent, T_i is the slope parameter and coefficient A_i is determined by the unit-normal condition. Model parameters (T_i, n_i) for several species of identified hadrons have been inferred from 5 TeV p -Pb spectrum data as described in Ref. [16]. A soft-component model function for unidentified hadrons can be defined as the weighted sum

$$\hat{S}_0(m_t) = \sum_i z_{0i} \hat{S}_{0i}(m_{ti}), \quad (4)$$

where the weights for charged hadrons follow $\sum_i z_{0i} = 1$. In the present context model function $\hat{S}_0(m_t)$ should not be confused with sphericity S_0 introduced in Ref. [3].

The unit-normal hard-component model is a Gaussian on $y_{t\pi} \equiv \ln[(p_t + m_{t\pi})/m_\pi]$ (as explained below) with exponential (on y_t) or power-law (on p_t) tail for larger y_t

$$\begin{aligned} \hat{H}_0(y_t) &\approx A \exp \left\{ -\frac{(y_t - \bar{y}_t)^2}{2\sigma_{y_t}^2} \right\} \quad \text{near mode } \bar{y}_t \\ &\propto \exp(-qy_t) \quad \text{for larger } y_t - \text{the tail,} \end{aligned} \quad (5)$$

where the transition from Gaussian to exponential on y_t is determined by slope matching [11]. The \hat{H}_0 tail density on p_t varies approximately as power law $1/p_t^{q+1.8} \approx 1/p_t^n$. Coefficient A (≈ 0.3) is determined by the unit-normal condition. Model parameters ($\bar{y}_t, \sigma_{y_t}, q$) are derived as described in App. A except as noted in the main text.

All spectra are plotted vs pion rapidity $y_{t\pi}$ with pion mass assumed. The motivation is comparison of spectrum hard components demonstrated to arise from a common underlying jet spectrum on p_t [11], in which case $y_{t\pi}$ serves simply as a logarithmic measure of hadron p_t with well-defined zero. $\hat{S}_0(m_t)$ in Eq. (4) is transformed to $y_{t\pi}$ via the Jacobian factor $m_{t\pi} p_t / y_{t\pi}$ to form $\hat{S}_0(y_{t\pi})$ for unidentified hadrons. $\hat{H}_0(y_t)$ in Eq. (5) is always defined on $y_{t\pi}$ as noted. In general, plotting spectra on a logarithmic rapidity variable provides improved access to important spectrum structure in the low- p_t interval where the majority of jet fragments appear.

C. p - p p_t spectrum data

Figures 1 and 2 (a,c) show the general relation between the TCM (solid) and ALICE data (points). The TCM is not the result of fits to individual spectra. The curves actually represent predictions derived from a self-consistent description of p - p spectra covering the energy interval 17 GeV to 13 TeV (Ref. [17] and App. A). The data/TCM ratios in (b,d) provide important information on biases resulting from V0M and SPD event sorting methods.

The TCM format of Figs. 3 and 4 then provides a more-differential decomposition of spectrum data into soft and hard components. Panels (a,c) show full data spectra (thin solid) in the normalized form $X(y_t)$ defined above that are directly comparable with soft-component model $\hat{S}_0(y_t)$ (bold dashed). Below 0.5 GeV/c ($y_t \approx 2$) the data curves closely follow the model. The same $\hat{S}_0(y_t)$ model is used for both event-selection methods.

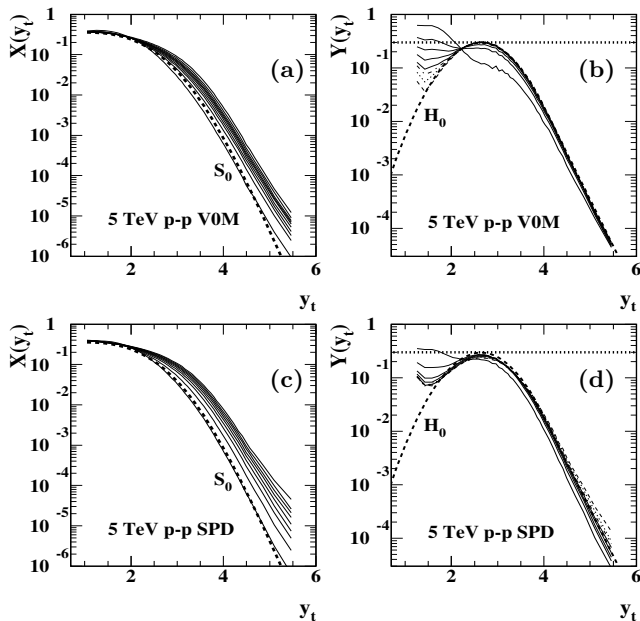


FIG. 3: Left: Normalized y_t spectra in the form $X(y_t)$ from ten (V0M) or nine (SPD) multiplicity classes of 5 TeV p - p collisions for V0M (a) and SPD (c) event selection. Right: Normalized spectrum hard components in the form $Y(y_t)$ for data in the left panels for V0M (b) and SPD (d) event selection. The bold dashed curves are TCM model functions.

Panels (b,d) show inferred data hard components $Y(y_t)$ defined by Eq. (2) (thin, several line styles) compared to TCM hard-component model $\hat{H}_0(y_t)$ (bold dashed). Deviations from $\hat{H}_0(y_t)$ below $y_t = 2$ appear in every p - p collision system (e.g. 200 GeV as reported in Ref. [10]). The horizontal dotted lines provide a check on proper normalization of hard-component model $\hat{H}_0(y_t)$. The data hard component for the lowest multiplicity class is not shown because there is in effect very little jet contribution to those events due to strong selection bias. Note that full spectra in panels (a,c) for the lowest n_{ch}

class are approximately consistent with $\hat{S}_0(y_t)$. The same $\hat{H}_0(y_t)$ model is used for both event-selection methods.

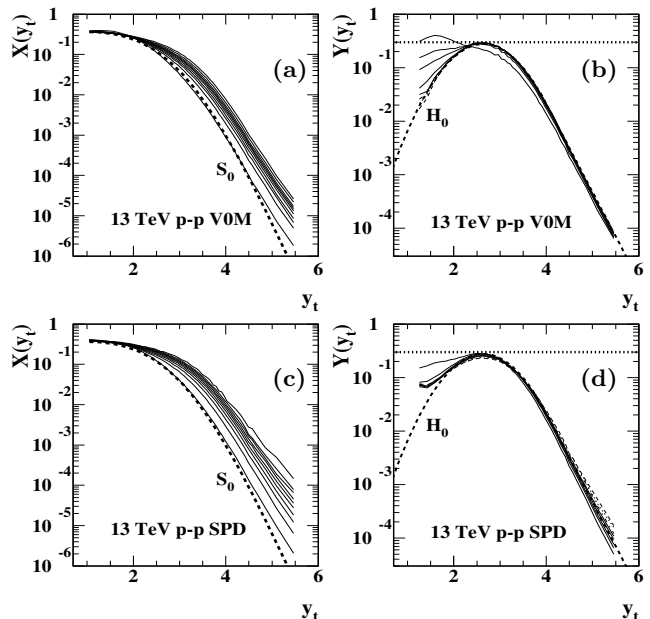


FIG. 4: Left: Normalized y_t spectra in the form $X(y_t)$ from ten multiplicity classes of 13 TeV p - p collisions for V0M (a) and SPD (c) event selection. Right: Normalized spectrum hard components in the form $Y(y_t)$ for data in the left panels for V0M (b) and SPD (d) event selection. The bold dashed curves are TCM model functions.

Although Ref. [3] states that p - p p_t spectra show “little energy dependence” both soft and hard components exhibit significant energy dependence as previously reported in Ref. [17]. The TCM parameters n (soft-component exponent) and q (hard-component exponent) vary systematically with $\log(\sqrt{s})$. The variation is apparent as shifts of $\hat{S}_0(y_t)$ and $\hat{H}_0(y_t)$ intercepts on y_t (at plot lower bounds) to larger values with increasing energy. The former may be related to increasing depth of the longitudinal splitting cascade on proton momentum fraction x with increasing energy [17], and the latter is certainly related to expected evolution of the underlying jet spectrum with increasing p - p collision energy [13].

D. Spectrum TCM parameter summary

Table I presents TCM parameters for 5 TeV and 13 TeV p - p collisions. Entries are grouped as soft-component parameters (T, n), hard-component parameters ($\bar{y}_t, \sigma_{y_t}, q$), hard/soft ratio parameter α and NSD (non-single-diffractive) soft density $\bar{\rho}_{sNSD}$. For unidentified hadrons soft component $\hat{S}_0(m_t)$ may be approximated by Eq.(3) for pions only with parameters as in Table I. Slope parameter $T = 145$ MeV is held fixed for all cases consistent with data. Its value is determined within a low- y_t interval where the hard component is negligible.

For the present analysis Eq. (3) was evaluated separately for pions, kaons and protons with $T_i = 140, 200$ and 210 MeV respectively. Those expressions were then combined to form $\hat{S}_0(m_t)$ via Eq. (4) with $z_{0i} = 0.82, 0.12$ and 0.06 respectively. For each energy the same exponent n was applied to three hadron species. Lévy exponent n values and hard-component q values are as reported in Table I.

$\bar{\rho}_{sNSD}$ values are derived from the universal NSD trend $\bar{\rho}_{sNSD} \approx 0.81 \ln(\sqrt{s}/10 \text{ GeV})$ inferred from spectrum and yield data. $\bar{\rho}_{0NSD}$ values are derived from the TCM relation $\bar{\rho}_0 \approx \bar{\rho}_s + \alpha \bar{\rho}_s^2$. The NSD $\bar{\rho}_0$ values can be compared with $\bar{\rho}_0 = 5.91$ and 7.60 for 5 and 13 TeV INEL > 0 events from Ref. [3] [above its Eq. (1)]. The 13 TeV number contrasts with 6.46 ± 0.19 in its Fig. 5 (center panel). Appendix A describes previous TCM analysis of 13 TeV p - p p_t spectrum data from Ref. [18].

TABLE I: p_t spectrum TCM parameters for 5 TeV and 13 TeV NSD p - p collisions within $\Delta\eta \approx 2$.

\sqrt{s} (TeV)	T (MeV)	n	\bar{y}_t	σ_{y_t}	q	100α	$\bar{\rho}_{sNSD}$	$\bar{\rho}_{0NSD}$
5.0	145	8.5	2.63	0.58	4.0	1.45	5.0	5.3
13.0	145	7.8	2.66	0.60	3.8	1.70	5.8	6.3

It should be noted that the α values for 5 TeV and 13 TeV in Table I are 0.0145 and 0.0170 whereas Table II includes values reported in Ref. [17] for alpha as 0.013 and 0.015. The earlier values were based on limited 13 TeV p - p spectrum data from Ref. [18]. The updated values better accommodate the much more complete spectrum data reported in Ref. [3]. The $\approx 12\%$ increase in α values is compatible with estimated uncertainties in Fig. 16 (left) of Ref. [17] but also favors a prediction of the $\alpha(\sqrt{s})$ trend based on measured p - p jet cross sections and fragmentation functions (dashed curve in that panel).

IV. p_t SPECTRUM BIASES AND EVOLUTION

V0M and SPD event-selection methods bias event structure (e.g. p_t spectra) in different ways. Biases are examined here relative to a TCM reference. The TCM for p - p collisions assumes linear superposition of parton-parton interactions consistent with basic QCD (e.g. published jet measurements). The TCM is not fitted to individual spectra; it serves as a fixed reference for comparison of biases from different event-selection methods.

A. Spectrum ratios vs n_{ch}

In its Figs. 2 and 3 Ref. [3] presents ratios of p_t spectra for ten n_{ch} classes to those for minimum-bias INEL > 0 ensemble averages for each of two event selection criteria. It is noted that “While at low p_T (< 0.5 GeV/c) the ratios exhibit a modest p_T dependence, for $p_T > 0.5$ GeV/c

they strongly depend on multiplicity and p_T .” It is possible to arrive at more-detailed quantitative conclusions using TCM-based techniques first reported in Ref. [10].

Figure 5 shows spectra from 13 TeV p - p collisions for V0M (left) and SPD (right) event classes and for data from Ref. [3] (solid) and corresponding TCM (dashed). The various spectra are in ratio to the TCM spectra for n_{ch} class 5 where 1-10 goes from higher to lower n_{ch} . The spectra have first been normalized by the corresponding soft-component density $\bar{\rho}_s$ as they appear in Fig. 4 (a,c).

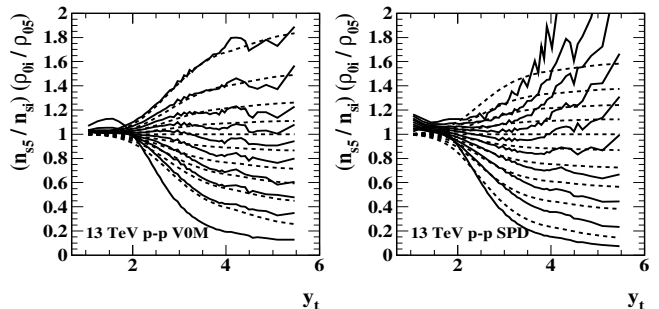


FIG. 5: Spectrum ratios for data (solid) and TCM (dashed) from 13 TeV p - p collisions in ratio to the TCM spectrum for event class V for V0M (left) and SPD (right) event selection.

The corresponding Figs. 2 and 3 in Ref. [3] show ratios of p_t spectra to a single minimum-bias INEL > 0 reference spectrum. As such the spectrum ratios include three sources of systematic variation: (a) mean event multiplicity varying from class to class, (b) varying jet contribution relative to charge multiplicity and (c) bias effects that are of major interest. It is then essentially impossible to sort out what cause produces which effect.

Figure 5 removes variation due to mean event multiplicity, but strong variation of jet contributions relative to total yield is still confused with bias effects. As a consequence of that plotting format, below $y_t = 2$ (0.5 GeV/c) spectra nearly coincide as a result of the chosen normalization and are nearly constant on y_t , qualitatively consistent with the observation in Ref. [3] (modulo distortions from selection bias discussed in the next subsection). Above that point the ratios vary strongly with n_{ch} and p_t , also qualitatively consistent with Ref. [3]. However, such variation is to be expected given that jet production varies approximately *quadratically* with n_{ch} .

Close examination of the left panel reveals that the data spectrum for the highest V0M n_{ch} class corresponds to the TCM (dashed) within statistics. Then with decreasing n_{ch} spectra are suppressed relative to the TCM at higher p_t but are enhanced at lower p_t . Correlated suppression and enhancement lead to trends in Fig. 12 where spectrum *integrals* adhere to the TCM trend $\bar{\rho}_h \propto \bar{\rho}_s^2$ for all event classes even as the spectrum hard components are significantly modified in shape with decreasing n_{ch} .

B. V0M and SPD biases relative to the TCM

Event sorting or selection in Ref. [3] is based on different angular acceptances denoted by acronym. SPD denotes tracklets (two hits plus vertex) within $|\eta| < 0.8$, the same angular acceptance as for the p_t spectra. V0M denotes a “forward estimator” with combined acceptances $\eta \in [2.8, 5.1]$ and $\eta \in [-3.7, -1.7]$ that is said to “minimize the possible autocorrelations introduced by the use of the mid-pseudorapidity estimator.” The term “autocorrelations” is here misused. The autocorrelation function (special case of cross-correlation function) is an established statistical method for analyzing time series [22]. A better term is *selection bias* wherein event selection is based on the same particle sample (e.g. mid-rapidity hadrons) as the object of study (mid-rapidity p_t spectra).

Figure 6 shows data/TCM ratios for 13 TeV p - p collisions and for V0M (left) and SPD (right) event classes. In contrast to Fig. 5 the systematic variation of jet yield relative to total yield is largely canceled in the data/TCM ratio. The same TCM reference is used for both selection methods. What remains is the bias effects of interest. The 5 TeV results are similar. The two methods bias spectra substantially but in *apparently* different ways. V0M for smaller multiplicities suppresses spectra at higher y_t but produces complementary enhancement at lower y_t . SPD for smaller multiplicities also suppresses higher y_t and enhances lower y_t , but for greater n_{ch} there is *apparently* strong enhancement for higher y_t whereas V0M produces no significant corresponding effect. However, spectrum *ratios* exaggerate structure at higher y_t while concealing important structure at lower y_t [17]. For example, compare these results with data-model *differences* in ratio to statistical errors (Z-scores) in Fig. 8.

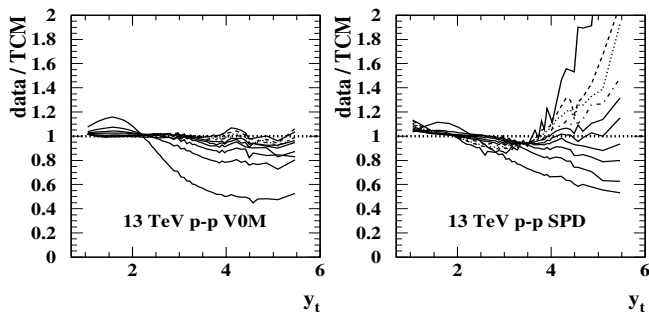


FIG. 6: Data/TCM spectrum ratios from 13 TeV p - p collisions for V0M (left) and SPD (right) event selection.

As can be seen in Figs. 3 and 4 (b,d) the physical process biased by event selection is jet production represented by the TCM spectrum hard component. The TCM hard-component reference has fixed exponent q corresponding to p_t power-law exponent n . The constant trend for the data/TCM ratio above $y_t = 4$ in Fig. 6 (left) is consistent with n or q independent of n_{ch} , whereas the result in Fig. 6 (right) is consistent with strong decrease of those parameters with increasing n_{ch} . See Figs. 9

(right) and 17 (left). The different forms of spectrum bias relating to V0M and SPD as indicated by Fig. 6 can thus be understood in terms of jet production.

Minimum-bias jet production near midrapidity arises from three processes: (a) separate parton splitting cascades within projectile protons resulting from inelastic scattering, (b) occasional large-angle scattering of cascade (participant) partons and (c) fragmentation of scattered participant partons to dijets. A proton splitting cascade (*event-wise* parton distribution function or PDF) is sensitive to initial conditions and fluctuates strongly from event to event [23]. Likewise, the fragment distribution within a jet (also a splitting cascade) fluctuates strongly from jet to jet. The biases indicated in Fig. 6 result from sorting the *same* minimum-bias INEL > 0 event population according to two different criteria.

Since V0M selection is derived from particle yields at higher η outside the acceptance for spectra it cannot significantly bias the jet formation process itself since most jets, near the lower bound of the jet spectrum, are derived from low- x partons appearing near midrapidity within a longitudinal cascade. However, V0M selection for low n_{ch} may influence the underlying jet spectrum resulting from the event-wise PDF, i.e. softening the jet spectrum. The result is a shift of the data hard component to lower y_t without changing its shape, consistent with Fig. 6 (left).

Since SPD selection is based on particle yields within the same acceptance as for p_t spectra it relates primarily to low- x partons *and* low-energy jets. It cannot significantly bias the event-wise PDF at larger x (or η) but can strongly bias the parton scattering and fragmentation process near midrapidity. Figure 6 (right) suggests that whereas lower SPD values produce a bias similar to V0M (softened jet spectrum), for higher SPD values the effective jet spectrum *and* mean fragmentation function are biased to harder distributions leading to evolution of the hard-component tail. The manifestation in the data/TCM *ratio* seems dramatic but a very small fraction of all particles is actually involved. Figures 3, 4 and 8 provide a more transparent picture of hard-component biases arising from V0M and SPD event selection.

The role of fluctuations warrants further consideration. It would be informative to have a 2D plot of event density on SPD vs V0M. Given the jet production scenario described above one may conjecture qualitatively that for large V0M yields (and hence event-wise PDF) the SPD event multiplicity and especially jet contribution is free to fluctuate strongly over a large range whereas the multiplicity *mean value* for fixed V0M remains modest as observed. In contrast, for large SPD yields the largest jet fluctuations are singled out, V0M is pinned to its highest value (V0M fluctuations are thus limited) and the multiplicity mean value for fixed SPD is large as observed. In Fig. 8 the most significant bias structure (the bipolar excursion on y_t) has maximum amplitude for the *lowest* values of V0M and SPD. The trend is consistent with a biased underlying jet spectrum (via the event-wise PDF).

C. Significance of data-model differences

Data/model spectrum ratios may exaggerate deviations at higher p_t compared to deviations at lower p_t . A more transparent representation is based on statistical-significance measures. The Z-score [24] compares data-model differences to their statistical uncertainties

$$Z_i = \frac{O_i - E_i}{\sigma_i}, \quad (6)$$

where O_i is an observation (e.g. spectrum data), E_i is an expectation (e.g. predictions derived from a model) and σ_i is the statistical uncertainty of the observation.

Figure 7 shows statistical errors σ_i (solid) accompanying published VOM and SPD spectrum data for 5 and 13 TeV p - p collisions which exhibit step-like structures. If used to process data within ratios those structures are injected into the result. Smooth approximations (dashed) are introduced to represent statistical errors without step-like structures. The approximated error curves are used for data-model comparisons below.

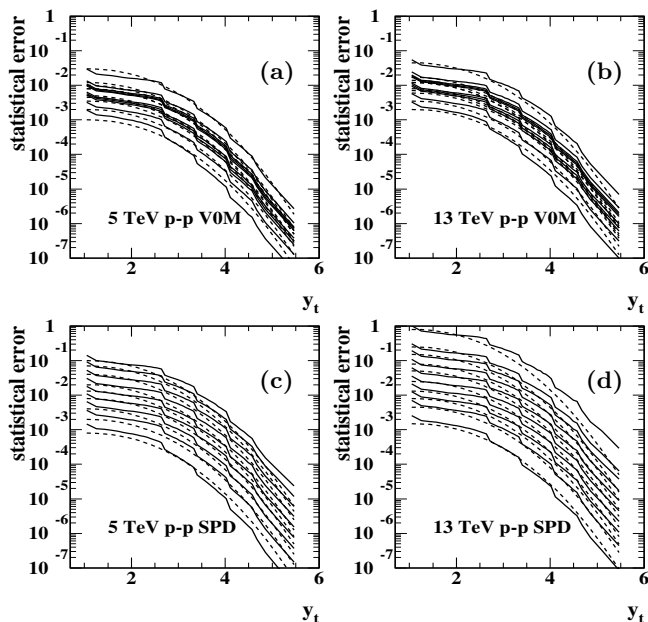


FIG. 7: Statistical errors (solid) as reported in Ref. [3] for 5 TeV (left) and 13 TeV (right) p - p collisions. To avoid the step-like structures in the data errors simple models (dashed, Gaussians on y_t) are used to approximate the error trends.

Figure 8 shows data-TCM differences in ratio to statistical uncertainties for 5 TeV (left) and 13 TeV (right) p - p collisions and for VOM (upper) and SPD (lower) event selection. Such Z-score results can be contrasted with data/TCM ratios as in Fig. 6. Whereas in the ratio format biases for VOM and SPD appear quite different, the Z-scores in Fig. 8 reveal the *statistical significance* of data-model deviations. Despite noticeable differences at higher p_t the most significant bias effects are similar.

The bias amplitude in terms of Z-scores seems to track with fraction of total cross section rather than with n_{ch} .

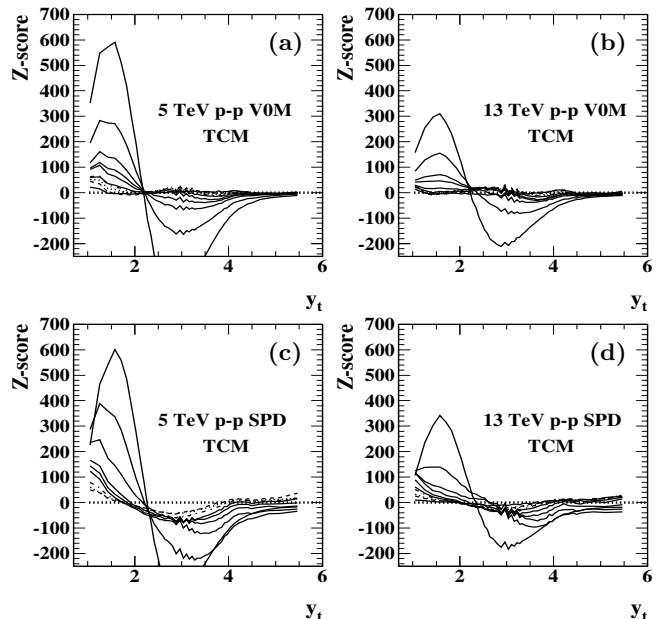


FIG. 8: Data-TCM differences in ratio to statistical errors (Z-scores) for 5 TeV (left) and 13 TeV (right) and for VOM event selection (upper) and SPD selection (lower). The highest multiplicity classes in each case are represented by solid, dashed, dotted and dash-dotted curves in descending order.

V. p_t SPECTRUM SHAPE MEASURES

Reference [3] analyzed the evolution of p_t spectrum shapes with varying charge multiplicity n_{ch} in two ways: (a) power-law model fits to spectra to infer trends for power-law exponent n and (b) variation of integrated yields within three p_t intervals compared to a minimum-bias reference as a function of n_{ch} . This section considers such shape-measure results in the context of the TCM.

A. Power-law fits to high- p_t intervals

Reference [3] fitted a power-law function to 13 TeV p - p spectra above 6 GeV/c ($y_t \approx 4.5$) to estimate exponents n vs n_{ch} for VOM and SPD events. A related result can be obtained without curve fitting via a logarithmic derivative applied directly to data hard components $Y(y_t)$ as in Figs. 3 and 4 (b,d) or $Y(p_t) = y_t Y(y_t) / m_t p_t$:

$$\begin{aligned} -\frac{d \ln[Y(y_t)]}{d y_t} &\rightarrow q \quad \text{for } y_t > 4.1 \\ -\frac{d \ln[Y(p_t)]}{d \ln(p_t)} &\rightarrow n \quad \text{for } y_t > 4.1. \end{aligned} \quad (7)$$

If $dn_{ch}/y_t dy_t \propto \exp(-qy_t)$ [high- y_t tail of $\hat{H}_0(y_t)$] then $dn_{ch}/p_t dp_t = (y_t/m_t p_t) dn_{ch}/y_t dy_t \propto 1/p_t^{q+2} \approx 1/p_t^n$.

$n \approx q + 2$ is a rough estimate, but $n \approx q + 1.8$ is established by direct comparison of results from Eq. (7) (upper and lower) for the same spectra. Power-law exponent n invoked by Ref. [3] should not be confused with TCM Lévy exponent n for soft component $\hat{S}_0(m_t)$.

Figure 9 (left) shows logarithmic derivatives vs y_t (thin solid) for eight n_{ch} classes of 13 TeV V0M p - p collisions. The bold dashed curve results from applying the same technique to TCM hard-component model $\hat{H}_0(p_t)$. Horizontal dotted lines represent values $n \approx q + 1.8$ expected for 5 (upper) and 13 (lower) TeV p - p collisions from TCM q energy trends related to Ref. [17] (see Table I). The crossed solid lines for $y_t = 2.65$ and $n = 1.8$ remind that while the mode of the hard component on y_t is near 2.65 (where the upper line of Eq. (7) would pass through zero) the mode on p_t is near $p_t = 0.5$ GeV/c ($y_t \approx 2$ where the lower line of Eq. (7) would pass through zero). See Fig. 20 (right) and associated text.

In this data format the spike artifacts common to all spectrum classes are most evident since differential measures are sensitive to short-wavelength structure. As noted, it may be that those artifacts arise from efficiency corrections derived from Monte Carlo data with more-limited statistics than the spectrum data themselves.

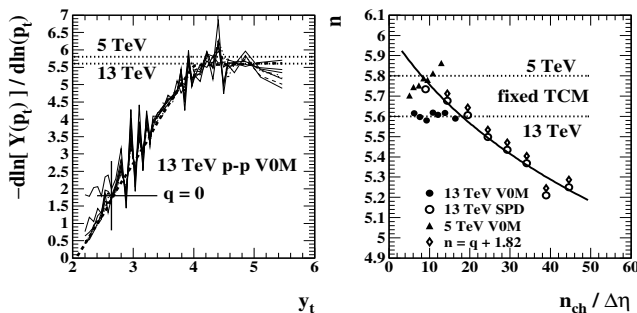


FIG. 9: Left: Logarithmic derivatives defined by Eq. (7) (second line, thin solid) for ten n_{ch} classes of 13 TeV p - p collisions and V0M events. The dashed curve is the same operation applied to TCM hard component $\hat{H}_0(p_t)$. The crossed solid lines are explained in the text. Right: Power-law exponents n obtained by averaging the last ten points in the left panel (i.e. $y_t > 4.1$, $p_t > 4.2$ GeV/c). Points corresponding to $n = q + 1.8$ with q from Fig. 17 (left) are raised by 0.02 for visibility. The curve is derived from Eq. (A2). Power-law exponent n should not be confused with TCM \hat{S}_0 exponent n .

Figure 9 (right) shows exponents n vs n_{ch} for three spectrum data types. The n values are in each case averages over the ten highest- y_t data points ($y_t > 4.1$ or $p_t > 4.2$ GeV/c) in the left panel. That limit is lower than the fit interval $p_t > 6$ GeV/c applied in Ref. [3]. However, the V0M results in the left panel indicate that the exponent trend is approximately constant down to $y_t = 4.1$, and the added points provide more-stable n values. The values for highest and lowest multiplicity classes are not plotted because of excessive noise in the log-derivative results. The V0M data trends on n_{ch} are

approximately constant, with values close to 5.60 (13 TeV) and 5.80 (5 TeV). The dotted lines correspond to TCM $\hat{H}_0(y_t)$ $q = 3.8$ for 13 TeV and 4.0 for 5 TeV related to Ref. [17] (see Table I). The SPD data trend varies strongly, decreasing (i.e. to harder spectra) with increasing n_{ch} . Those trends are consistent with spectrum data trends in Figs. 1 and 2 (b,d) showing deviations from fixed TCM references. The solid curve for 13 TeV SPD data is derived from Eq. (A2) with $n = q + 1.8$. The 5 TeV SPD data are more scattered than other data trends and are thus omitted to improve visual access to the 13 TeV SPD trend relevant to Fig. 5 of Ref. [3].

In its summary Ref. [3] concludes “...within uncertainties, the functional form of n as a function of $\langle dN_{ch}/d\eta \rangle$ is the same for the two multiplicity estimators [V0M and SPD] used in this analysis. Moreover, n is found to decrease with $\langle dN_{ch}/d\eta \rangle$.” The results in Fig. 9 contradict that conclusion: The power-law trend is dramatically different for V0M and SPD, and n does not decrease with charge density for V0M event selection. The contrast between V0M and SPD event selection is most evident in Fig. 6. In the left panel the effective exponent at high p_t relative to the fixed TCM value is itself fixed (the ratio is approximately constant above $y_t = 4$). The right panel shows dramatic variation of the effective SPD exponent from high (soft) to low (hard) with increasing n_{ch} .

B. Spectrum response to selection bias

Figures 4 and 6 of Ref. [3] deal with other manifestations of selection bias in p_t spectrum structure. Figure 6 compares yields integrated within three specific p_t intervals Δp_t for ten multiplicity classes in ratio to yields in the same intervals from the INEL > 0 minimum-bias class. The resulting data trends are compared to a linear $y = x$ trend corresponding to *no change in spectrum shape* with n_{ch} . Figure 4 compares V0M and SPD spectra for nearly-equal charge densities $\bar{\rho}_0 \approx 20$. Ratio SPD/V0M drops to 0.85 near 4 GeV/c for both 5 and 13 TeV spectra. What follows is an effort to understand systematics details and provide a physical interpretation.

Figure 10 (left) shows integrated yields $n_{ch}(\Delta p_t)$ for three p_t intervals from spectra for ten n_{ch} classes of SPD and V0M events in ratio to yields $n_{ch,INEL}(\Delta p_t)$ in the same intervals (points) from a 13 TeV TCM p_t spectrum defined on data p_t values with $\bar{\rho}_0 = 7.60$ as for INEL > 0 events in Ref. [3]. The solid lines are TCM references resulting from the same method applied to TCM spectra defined “on a continuum” (i.e. on 100 equal-spaced y_t points extending down to $y_t = 0$). Soft and hard TCM model functions do not vary with n_{ch} . The different slopes of the TCM lines result only from the different fractions of soft and hard components in each p_t interval. The log-log plot format ensures that suppression at smaller n_{ch} is as visible as enhancement at larger n_{ch} . The effects of selection bias are indicated by deviations of data from the TCM trends, *not* from the $y = x$ dot-

ted line (that assumes no change in jet production). As for Fig. 5 above or Figs. 2 and 3 in Ref. [3] distinction should be maintained between variations due to generic jet trends and bias effects relative to those variations.

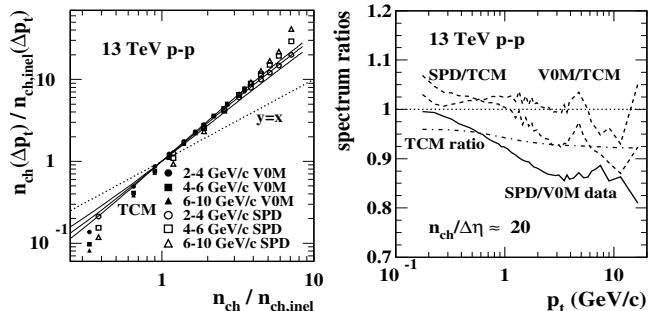


FIG. 10: Left: Ratios of yields (points) from p_t spectra within three Δp_t intervals for ten p - p V0M or SPD event classes to yields from the same intervals and from INEL > 0 events. The independent variable is mean event multiplicity n_{ch} in ratio to INEL > 0 mean multiplicity $n_{ch,INEL}$. The solid reference curves result from the same method applied to TCM spectra defined on a y_t continuum. Right: Ratios of data spectra to corresponding TCM references for class II of V0M data and class VII of SPD data (dashed), which both approximately correspond to $\bar{\rho}_0 = 20$. The solid curve is SPD/V0M data spectra compared directly in ratio, reportedly demonstrating that SPD is softer than V0M for the same charge multiplicity. However, the corresponding TCM ratio (dash-dotted) demonstrates that most of the deviation from unity is simply due to the V0M vs SPD multiplicity difference. The two panels relate to Figs. 6 and 4 respectively of Ref. [3].

Several features are apparent. For V0M events points for different Δp_t at higher n_{ch} approximately coincide, consistent with Fig. 6 (left) where the ratios for higher n_{ch} are nearly flat on p_t . In contrast, higher- n_{ch} points for SPD vary strongly with p_t interval Δp_t , consistent with Fig. 6 (right). For lowest n_{ch} classes there is strong suppression below the TCM references for both V0M and SPD, also consistent with spectrum ratios in Fig. 6, but suppression for V0M is significantly greater than for SPD.

Figure 10 (right) shows 13 TeV data/TCM spectrum ratios (dashed) for class II V0M/TCM and class VII SPD/TCM, data/data ratio SPD/V0M (solid) that appears in Fig. 4 of Ref. [3] and the corresponding ratio of TCM spectra (dash-dotted). Commenting on the SPD/V0M spectrum ratio in its Fig. 4 (identical to the solid curve here) Ref. [3] states that “For transverse momenta within 0.5-3 GeV/c the spectra [sic] for the [V0M] multiplicity class II is harder than that for the [SPD] multiplicity class VII.” However, the 5% difference in $\bar{\rho}_0$ for V0M (20.5) and SPD (19.5) plays a significant role as indicated by the TCM ratio (dash-dotted). Since TCM model functions \hat{S}_0 and \hat{H}_0 are fixed, charge density $\bar{\rho}_0$ determines the TCM spectrum shape. The TCM ratio demonstrates the effect of the V0M vs SPD multiplicity difference: at least half of the SPD/V0M ratio deviation from unity arises from the difference in $\bar{\rho}_0$. Absent de-

tailed comparisons with a model the term “harder” may mean a modified jet fragment distribution or simply more or less jet production according to $\bar{\rho}_h \approx \alpha \bar{\rho}_s^2$.

One should also note that class VII is comparatively low n_{ch} for SPD whereas class II is relatively high n_{ch} for V0M. Given the trends in Fig. 8 (b,d) one should then expect a substantial difference in *bias* for the two cases, as observed. Concerning the short-wavelength structure, the peaks near 5 GeV/c in the data/TCM ratios certainly correspond to the bipolar structure near $y_t = 4.4$ in Fig. 9 (left) that is common to all n_{ch} classes and therefore most probably results from the inefficiency correction. That structure then cancels in the SPD/V0M data ratio even though the spectra are from quite different event classes.

C. Spectrum running integrals

In Sec. IV of Ref. [10] running integrals of y_t spectra were the basis for discovery of the two-component structure of 200 GeV p - p p_t spectra without *a priori* assumptions. It was observed that spectra normalized not with total charge density $\bar{\rho}_0$ but with a “soft component” $\bar{\rho}_s$ defined as the root of $\bar{\rho}_0 = \bar{\rho}_s + \alpha \bar{\rho}_s^2$ with $\alpha \approx O(0.01)$ coincided below $y_t = 2$ ($p_t \approx 0.5$ GeV/c) within data uncertainties and that the endpoints of spectrum running integrals also followed a trend consistent with the above quadratic equation. The same approach is applied here to 13 TeV p - p spectrum data. One purpose is demonstration that the p_t spectrum TCM is *required* by p - p data for any energy, is not imposed *a priori*.

Figure 11 shows running integrals of y_t spectra for ten n_{ch} classes of 13 TeV p - p collisions each for V0M (left) and SPD (right) event selection criteria derived from data (solid) and TCM (dashed) spectra. Spectra are normalized by $\bar{\rho}_s$ inferred from $\bar{\rho}_0$ reported in Ref. [3] using the quadratic equation defined above with $\alpha = 0.017$ for 13 TeV, 12% higher than reported in Ref. [17]. The uncorrected spectrum running integrals are then defined as

$$\Sigma'(p_t; n_{ch}, p_{t,cut}) = \frac{1}{\bar{\rho}_s} \int_{p_{t,cut}}^{p_t} dp'_t p'_t \bar{\rho}_0(p'_t; n_{ch}). \quad (8)$$

Note that a factor p'_t in the integrand is required in order to be consistent with the definition of $\bar{\rho}_0(y_t; n_{ch})$ in Eq. (1). Running integrals on data p_t values within the ALICE p_t acceptance can be simply corrected for incomplete p_t acceptance. The correction is addition of estimated $1 - \xi$ corresponding to $p_{t,cut} \approx 0.15$ GeV/c (see Fig. 14, left and related text).

The corrected data running integrals can be expressed in TCM form on y_t as

$$\Sigma(y_t) = \Sigma_s(y_t) + \Sigma_h(y_t). \quad (9)$$

As in Ref. [10] the corrected data running integrals coincide below $y_t = 2$ ($p_t \approx 0.5$ GeV/c) within data uncertainties then separate and achieve saturation above $y_t = 4.0$ ($p_t \approx 3.8$ GeV/c). Running integral $\Sigma_0(y_t)$

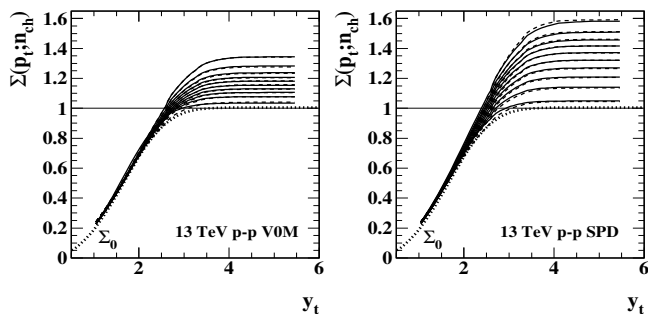


FIG. 11: Running integrals for data (solid) and TCM (dashed) p_t spectra from 13 TeV p - p collisions and for V0M (left) and SPD (right) event selection. Running integrals have been corrected for incomplete p_t acceptance as described in the text. The bold dotted curve corresponds to model $\hat{S}_0(y_t)$.

(bold dotted) of TCM soft component $\hat{S}_0(y_t)$ is defined as the limit of data running integrals as $n_{ch} \rightarrow 0$ where $\Sigma_h(y_t) \rightarrow 0$. The functional form of $\hat{S}_0(y_t)$ given by Eqs. (3) and (4) is then observed to generate the required limiting form of $\Sigma_0(y_t)$ within data uncertainties. $\Sigma_0(y_t)$ saturates at 1 by definition. The same form is used for V0M and SPD data.

The data trends in Fig. 11 demonstrate the following: (a) The shape of data soft component $\Sigma_s(y_t)$ does not vary significantly with n_{ch} , is consistent with $\Sigma_0(p_t)$. (b) The complementary data hard components $\Sigma_h(y_t; n_{ch})$ are consistent with an $\text{erf}(y_t)$ function as running integral, demonstrating that data *spectrum* hard components are similarly-shaped peaked distributions with mode near $y_t = 2.7$ ($p_t \approx 1$ GeV/c) as demonstrated in Ref. [10]. It is then of interest to examine the n_{ch} trend of the data running-integral endpoints for TCM consistency.

Figure 12 shows running-integral endpoints vs $\bar{\rho}_s$ for 5 TeV (left) and 13 TeV (right) derived from data spectra for V0M (solid dots) and SPD (open circles) event selection. The result for uncorrected spectra is $\xi + x(n_s)$. The inefficiency correction is then $1 - \xi \approx 0.16$ for the TCM defined on SPD p_t values (dashed lines) as noted.

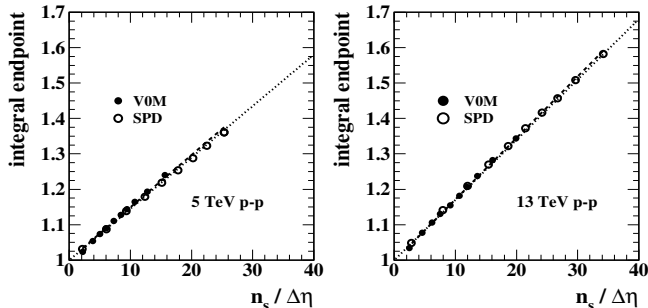


FIG. 12: Endpoints of data running integrals in Fig. 11 for V0M (solid dots) and SPD (open circles) and for 5 TeV (left) and 13 TeV (right) p - p collisions. The dashed lines are TCM endpoints on SPD p_t values. The dotted lines are TCM trends $1 + x(n_s) \rightarrow 1 + \alpha \bar{\rho}_s$ with $\alpha = 0.017$ (0.0145) for 13 (5) TeV.

Those results demonstrate *experimentally* the precise quadratic relation between hard and soft data components: (a) All spectra coincide precisely for $p_t < 0.5$ GeV/c given normalization via $\bar{\rho}_s$ as computed from measured $\bar{\rho}_0$ and (b) corrected-running-integral endpoints fall along straight-line loci $1 + \alpha \bar{\rho}_s$ (dotted lines) with $\alpha \bar{\rho}_s \approx x(n_s)$. The endpoint trends in turn accurately indicate the fractional contribution $x/(1+x)$ of jet fragments to total spectra. For the highest multiplicity classes $x \approx 0.5$ and 33% of hadrons are jet fragments.

In terms of TCM model functions, spectrum data demonstrate that one spectrum component scales linearly with $\bar{\rho}_s$ at lower p_t and that a second component scales *quadratically* with $\bar{\rho}_s$ at higher p_t . The p_t structures of the data components vary little with n_{ch} . Running integrals provide a less-sensitive way to probe spectrum *details* compared to Figs. 3 and 4. However, there are no assumptions about spectrum structure, per Ref. [10]. It is notable that the straight-line trends in Fig. 12 are followed down to the lowest event multiplicities although the data hard components are substantially biased there. The present study demonstrates that the p_t spectrum TCM, with its quadratic relation between soft and hard components, is *necessary* to describe 13 TeV p_t spectra (modulo biases described and interpreted in Sec. IV).

VI. p - p ENSEMBLE \bar{p}_t SYSTEMATICS

Ensemble-mean \bar{p}_t data are inferred from hadron spectra via integration. The \bar{p}_t values in Ref. [3] are obtained by integrating over $p_t \in [0.15, 10]$ GeV/c. Accurate values corresponding to ideal spectrum data could be obtained by extrapolating data spectra with a reliable spectrum model. Values obtained with unextrapolated spectra may be strongly biased, and correct interpretation of biased experimental \bar{p}_t values may be difficult. This section demonstrates how to relate a TCM reference to biased \bar{p}_t values obtained from spectrum data. The resulting bias is here estimated and corrected.

Reference [25] reported a comprehensive analysis of \bar{p}_t data vs event multiplicity for p - p , p -Pb and Pb-Pb collision systems. The strong increase of \bar{p}_t with n_{ch} for p - p collisions was there interpreted in terms of color reconnection as modeled within the PYTHIA Monte Carlo. The data trends were said to “pose a challenge to most of the existing models.” A TCM analysis of the same data was presented in Ref. [26]. The observed \bar{p}_t vs n_{ch} trends were found to be consistent with the jet (hard component) contribution to hadron production in all cases.

Reference [3] introduces sphericity measure S_0 intended to select more- or less-“jetty” events according to its value. Variation of jet production in a given event sample is expected to bias the \bar{p}_t vs n_{ch} trend. It is noted that as S_0 decreases \bar{p}_t increases, possibly due to an increased jet contribution to spectra as anticipated. In addition to biases resulting from incomplete p_t acceptance and from V0M and SPD event selection methods, biases

from event selection via sphericity S_0 are considered.

A. Ensemble \bar{p}_t TCM for p-p collisions

The TCM for ensemble-mean \bar{p}_t data from p - p collisions is summarized. It is assumed that due to incomplete p_t acceptance (lower bound $p_{t,cut} \approx 0.15$ GeV/c) only a fraction $\xi < 1$ of the p_t spectrum soft component is accepted. It is also evident that for such a low cutoff value the entire spectrum hard component is accepted. The \bar{p}_t values obtained from TCM model functions as defined by Table I are as follows: For models defined on the continuum ($\xi \approx 1$) the mean values are $\bar{p}_{ts} \approx 0.48$ GeV/c and $\bar{p}_{th} \approx 1.39$ GeV/c. For models defined on spectrum data p_t values the mean values are $\bar{p}_{ts} \approx 0.58$ GeV/c (corresponding to $\xi \approx 0.84$) and $\bar{p}_{th} \approx 1.38$ GeV/c.

The TCM for charge densities averaged over some angular acceptance $\Delta\eta$ (1.6 for $|\eta| < 0.8$ as in Ref. [3]) is

$$\begin{aligned}\bar{\rho}_0 &= \bar{\rho}_s + \bar{\rho}_h & (10) \\ &= \bar{\rho}_s[1 + x(n_s)], \\ \frac{\bar{\rho}'_0}{\bar{\rho}_s} &= \frac{n'_{ch}}{n_s} = \xi + x(n_s),\end{aligned}$$

where $x(n_s) \equiv \bar{\rho}_h/\bar{\rho}_s \approx \alpha\bar{\rho}_s$ is the p - p ratio of hard-component to soft-component yields [10] and $\alpha(\sqrt{s})$ is defined in Ref. [17]. $\bar{\rho}'_0$ is an *uncorrected* charge density corresponding to incomplete p_t acceptance with $\xi < 1$.

The TCM for extensive ensemble-mean *total* p_t integrated within some angular acceptance 2π and $\Delta\eta$ from p - p collisions for given (n_{ch}, \sqrt{s}) can be expressed as

$$\begin{aligned}\bar{P}_t &= \bar{P}_{ts} + \bar{P}_{th} & (11) \\ &= n_s\bar{p}_{ts} + n_h\bar{p}_{th}.\end{aligned}$$

The conventional *intensive* ratio of extensive quantities

$$\frac{\bar{P}'_t}{n'_{ch}} \equiv \bar{p}'_t \approx \frac{\bar{p}_{ts} + x(n_s)\bar{p}_{th}(n_s)}{\xi + x(n_s)} \quad (12)$$

(assuming $\bar{P}'_{ts} \approx \bar{P}_{ts}$ [27])² in effect partially cancels dijet manifestations represented by ratio $x(n_s)$ that may be of considerable interest. The alternative ratio

$$\begin{aligned}\frac{n'_{ch}}{n_s}\bar{p}'_t &\approx \frac{\bar{P}_t}{n_s} = \bar{p}_{ts} + x(n_s)\bar{p}_{th}(n_s) & (13) \\ &\approx \bar{p}_{ts} + \alpha(\sqrt{s})\bar{\rho}_s\bar{p}_{th}(n_s, \sqrt{s})\end{aligned}$$

preserves the simplicity of Eq. (11) and provides a convenient basis for testing the TCM hypothesis precisely.

² Because of the additional factor p'_t in $\bar{P}'_{ts} = \int_{p_{t,cut}}^{\infty} dp'_t p'^2_t \bar{\rho}_s(p'_t)$ the effect of the low- p_t cutoff is minimal and $\bar{P}'_{ts} \approx \bar{P}_{ts}$.

B. Sphericity event selection

Reference [3] studies ensemble \bar{p}_t trends vs sphericity

$$S_0(\%) = 100 \times \frac{\pi^2}{4} \min_{\hat{n}_s} \left(\frac{\sum_i |\vec{p}_{t,i} \times \hat{n}_s|}{\sum_i \vec{p}_{t,i}} \right)^2 \in [0, 100], \quad (14)$$

where \hat{n}_s is a unit vector varied to minimize S_0 . Limit 0% would result for a single p_t vector. Limit 100% would result for an infinite number of p_t vectors uniformly distributed on azimuth with *equal magnitudes*, in which case the quantity in parenthesis becomes $(1/\pi) \int_0^\pi d\phi \sin(\phi) = 2/\pi$. Events are sorted into ten sphericity classes with the intent to identify events based on the particle fraction arising from jets, i.e. the event “jettiness.”

C. ALICE ensemble \bar{p}_t results

Figure 13 (left) shows uncorrected (biased) ensemble \bar{p}'_t values vs n_{ch} (thin solid) from 13 TeV p - p collisions for ten classes of sphericity S_0 . According to Ref. [3] uncorrected \bar{p}_t is determined within acceptance $p_t \in [0.15, 10]$ GeV/c but n_{ch} is corrected by extrapolation to zero. The bold dash-dotted curve is a simple unweighted average of those spectra. As a result of the incomplete p_t acceptance the \bar{p}_t values are biased upward as for \bar{p}'_t in Eq. (12) with $\xi \approx 0.84$. The method of event selection on n_{ch} is based on n_{ch} appearing in angular acceptance $|\eta| < 0.8$ (i.e. SPD). The solid dots and open circles are \bar{p}_t values obtained from TCM spectra defined on a “continuum” (100 points equally spaced on $y_t \in [0, 6]$) for V0M and SPD n_{ch} which are then unbiased ($\xi \approx 1$). The dashed curves are TCM trends for 5 and 13 TeV described by Eq. (12) with $\xi = 1$ and hard component $\bar{p}_{th}(n_s) = 1.39$ GeV/c fixed. The open squares are the TCM defined on SPD data p_t values and integrated without extrapolation (i.e. are biased). The open triangles are from 13 TeV SPD p_t spectra reported in Ref. [3] also integrated without extrapolation (biased). The \bar{p}_t bias for uncorrected data is about 0.1 GeV/c (open squares vs upper dashed curve), consistent with Fig. 14 (left).

Figure 13 (right) shows the same data and curves (with the exception of sphericity-related curves, see Fig. 15) in the form of Eq. (13). The TCM trends follow straight-line loci whose *slopes* are determined by the spectrum jet contribution, controlled in this case by parameter α . The TCM defined on data points (open squares) and 13 TeV data SPD \bar{p}_t values (open triangles) have been corrected according to Eq. (13) with $\xi \approx 0.84$ in Eq. (10) (see below). The dashed lines are Eq. (13) with $\bar{p}_{ts} = 0.48$ GeV/c and $\bar{p}_{th} = 1.39$ GeV/c as described in Sec. VI A.

Figure 14 (left) shows the consequence of an incomplete p_t acceptance for calculation of \bar{p}_t per Ref. [27]. The solid curve is the running integral of $1 - \hat{S}_0(p_t)$ that determines the inefficiency parameter ξ as a function of spectrum lower bound $p_{t,cut}$, the fraction of $\hat{S}_0(p_t)$ that survives the cut. The lowest hatched band indicates

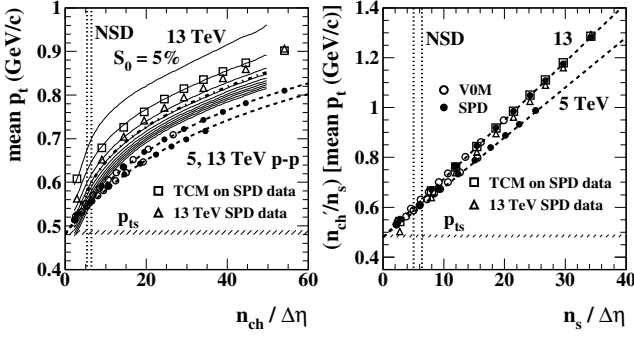


FIG. 13: Left: Ensemble-mean \bar{p}_t vs n_{ch} trends for 13 TeV events (thin solid) vs sphericity S_0 . The dash-dotted curve is an unweighted mean of those curves. The open triangles are \bar{p}_t from 13 TeV SPD data. The open squares are from uncorrected TCM spectra on data p_t values. The open and solid circles are the TCM “on a continuum” (see text). The dashed curves are TCM Eq. (12). Right: \bar{p}_t vs n_{ch} trends in the left panel converted per Eq. (13) with $\xi = 1$ for dots and circles and 0.84 for open squares and open triangles (corrected).

\bar{p}_t soft component $\bar{p}_{ts} \approx 0.48$ GeV/c determined from TCM fixed spectrum soft-component $\hat{S}_0(y_t)$ with no cutoff. $\bar{p}'_{ts} = \bar{p}_{ts}/\xi$ (dashed) is the biased \bar{p}_t soft component resulting from the cutoff. For cutoff $p_{t,cut} \approx 0.15$ GeV/c in Ref. [3] $\xi \approx 0.84$ (as in the previous paragraph) and $\bar{p}'_{ts} \approx 0.58$ GeV/c, i.e. about 0.1 GeV/c higher than the unbiased value. The right panel is explained below.

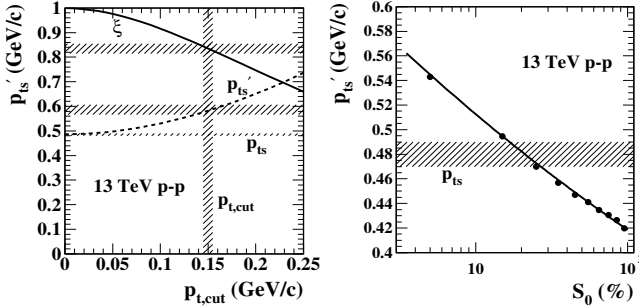


FIG. 14: Left: Fraction ξ (solid) of TCM soft component $\hat{S}_0(y_t)$ integrated above cutoff $p_{t,cut}$ and biased $\bar{p}'_{ts} = \bar{p}_{ts}/\xi$ (dashed). For nominal acceptance cut $p_{t,cut} \approx 0.15$ GeV/c $\xi \approx 0.84$ and $\bar{p}'_{ts} \approx 0.58$ GeV/c (hatched bands). Right: Biased \bar{p}'_{ts} vs sphericity S_0 (in percent) for corrected \bar{p}_t vs n_{ch} trends compared to $\bar{p}_{ts} \approx 0.48$ GeV/c (hatched band). Note that symbol \bar{p}'_{ts} represents different bias sources in the two panels – low- p_t acceptance cutoff vs sphericity S_0 .

Figure 15 (left) shows \bar{p}_t vs n_{ch} data trends in Fig. 13 (left) as they vary with sphericity S_0 (thin solid), the unweighted ensemble average (bold dash-dotted) and the TCM on 13 TeV SPD data p_t values (open squares) transformed according to Eq. (13) with $\xi \approx 0.84$ that can be compared with Fig. 13 (right). The open triangles are 13 TeV SPD data \bar{p}_t values treated the same. In this plotting format it is evident that for most data spectra the

primary variation with sphericity S_0 is soft-component mean \bar{p}_{ts} (y -axis intercepts in this plot) since the jet contribution (i.e. \bar{p}_{th}), determining slopes in this format, shows little variation with S_0 . The upper dotted line is $0.48 + 1.39\alpha\bar{\rho}_s$ consistent with TCM $\bar{p}_{ts} = 0.48 \pm 0.01$ GeV/c and $\bar{p}_{th} = 1.39 \pm 0.015$ GeV/c. The lower dotted line with $\bar{p}_{ts} = 0.42$ GeV/c and $\bar{p}_{th} = 1.30$ is consistent with the lowest S_0 curve for $\bar{\rho}_s > 15$.

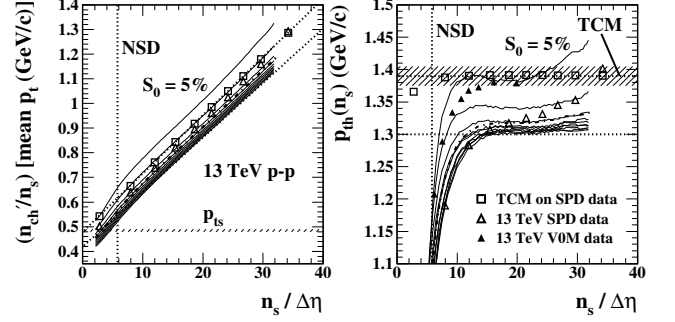


FIG. 15: Left: 13 TeV \bar{p}_t vs n_{ch} data vs sphericity S_0 (thin solid, dash-dotted) from Fig. 13 (left) transformed and corrected via Eq. (13) with $\xi \approx 0.84$. The open squares are the corrected 13 TeV TCM on data p_t values from Fig. 13 (right). \bar{p}_{ts} is derived from the TCM $\hat{S}_0(y_t)$ model function. Right: \bar{p}_t hard component $\bar{p}_{th}(n_s)$ derived from the contents of the left panel via Eq. (13). For the S_0 data $\bar{p}_{ts} \rightarrow \bar{p}'_{ts}(S_0)$ values from Fig. 14 (right) are used in Eq. (13). The dotted lines in left and right panels indicate the TCM trend (upper) and the lowest of the S_0 curves above $\bar{\rho}_s = 15$.

Figure 14 (right) shows empirically-determined biased soft-component values \bar{p}'_{ts} for the individual $\bar{p}_t(n_{ch})$ trends in Fig. 15 (left). The estimated values are simply described by the power-law expression $\bar{p}'_{ts}(S_0) \approx [0.048/S_0(\%)]^{0.088}$ GeV/c (straight line) over the entire S_0 range. The hatched band denotes the unbiased soft-component mean $\bar{p}_{ts} \approx 0.48$ GeV/c. The bias in this instance is not due to a p_t cutoff (which has been corrected), is instead the result of the imposed S_0 condition. The two points above the hatched band thus do not “cause” the two elevated trends in Fig. 15 (right).

Figure 15 (right) shows $\bar{p}_{th}(n_s)$ inferred from data in the left panel via Eq. (13) (second line) with $\bar{p}'_{ts}(S_0)$ taken from Fig. 14 (right) for each sphericity class. The value 1.39 GeV/c (hatched band) is just the \bar{p}_{th} corresponding to the 13 TeV TCM hard-component $\hat{H}_0(y_t)$ in Sec. IIIB. The adopted criterion for determining \bar{p}_{ts} values in Fig. 14 (right) is a requirement that $\bar{p}_{th}(n_s)$ trends be as level as possible above $\bar{\rho}_s = 15$, consistent with a constant $\bar{p}_{th}(n_s)$ trend in Eq. (13) reflecting the TCM. The horizontal dotted lines are the dotted lines at left transformed to obtain $\bar{p}_{th}(n_s)$ according to Eq. (13).

Deviations from the TCM reference in Fig. 15 (right) could in general carry significant new information about collision dynamics. However, the data mainly indicate that while jet production increases about 30-fold over the interval $\bar{\rho}_s \in [6, 33]$ it continues to follow the observed

$\bar{p}_h \propto \bar{p}_s^2$ trend precisely no matter what the value of S_0 .

The comparison between V0M and SPD \bar{p}_{th} values indicates that the SPD hard component mean p_t is biased down by almost 0.1 GeV/c *independent of* S_0 . The effect is evident in Fig. 6 in that the data trend on y_t for higher n_{ch} and for V0M is flat (i.e. agreeing with the TCM) whereas for SPD the hard component is shifted down on y_t (hence the tilt). Thus, for large SPD n_{ch} the high- p_t tail is hardened while the main part of the hard component is softened. Trends for higher S_0 (thin solid) agree with the basic SPD data. Only the lowest two S_0 values show significant hardening of the hard component.

Information carried by p_t spectra sorted by S_0 thus has three contributions: (a) bias of \bar{p}_{ts} as in Fig. 14 (right) indicates bias of the spectrum *soft* component in response to imposition of an azimuthal (a)symmetry condition via S_0 , (b) bias of the spectrum hard component in the form of strong modification of the hard-component shape with low n_{ch} condition as in Fig. 8 resulting in lower \bar{p}_t *independent* of S_0 , and differently for V0M and SPD, and (c) minor modification of the jet contribution to \bar{p}_t varying with S_0 as in Fig. 15 (right). Note that for the SPD data used in the S_0 study the *absolute* jet production increases (relative to NSD p - p collisions) by ≈ 30 -fold because of the n_{ch} variation (see Fig. 7 of Ref. [3]) while the largest effect of S_0 variation on the jet-related \bar{p}_t hard component is less than 10% (see Fig. 15, right).

D. ALICE ensemble \bar{p}_t summary

Results in this section suggest several conclusions: (a) The basic S_0 -related \bar{p}_t data in Fig. 13 (left) (thin solid) are strongly biased by the incomplete p_t acceptance (i.e. lower bound $p_{t,cut}$). The TCM results in the same panel illustrate the consequence of determining \bar{p}_t by integration down to zero p_t . In contrast, integrating TCM spectra on data p_t values (open squares, with cutoff) is close to (but not equal to) integrating spectra from Ref. [3] without extrapolation (open triangles).

(b) The $p_{t,cut}$ bias can be removed via Eq. (13) as shown in Fig. 13 (right). The biased TCM data in the left panel (open squares) are then in good agreement with unbiased TCM data in the right panel. The bias correction relies on estimating efficiency $\xi \approx 0.84$ based on a TCM soft-component model that provides good data descriptions down to 0.15 GeV/c as demonstrated in Sec. III C.

(c) The conventional \bar{p}_t ratio format of Eq. (12) and Fig. 13 (left) mixes two distinct physical mechanisms and is therefore difficult to interpret. Aside from bias corrections the data format corresponding to Eq. (13) and Fig. 13 (right) provides a clear distinction between \bar{p}_t data soft and hard components, especially some differential features of the isolated jet contribution $\bar{p}_{th}(n_s)$.

(d) Even with complete p_t acceptance the data spectra from Ref. [3] are still strongly biased by the event selection methods, both SPD *and* V0M, as illustrated by comparison with fixed (not fitted) TCM spectra in

Sec. II B (ratios in right panels). With demand for lower n_{ch} , spectra for any S_0 are increasingly softened leading to decreased \bar{p}_t relative to the TCM trend in Fig. 13 (left) (compare open squares and open triangles) and Fig. 15 (left, note the strong drop-off near and below the NSD \bar{p}_s value). The effect is most apparent in Fig. 15 (right) because $\bar{p}_{th}(n_s)$ corresponds to slopes in the left panel.

(e) Event selection via sphericity S_0 was intended primarily to bias jet production [3]. Data indicate that S_0 instead biases the spectrum soft component as evident from the nearly-linear trends in Fig. 15 (left) where the slopes (jet contribution) vary little while the y -axis intercepts (soft component) vary strongly according to a simple power-law trend shown in Fig. 14 (right). The origin of the bias is simple to identify. Large values of S_0 favor uniform azimuth distributions of *nearly-equal* p_t values. That condition then biases against higher- p_t contributions to the soft component which reduces \bar{p}_{ts} . Strong S_0 bias of \bar{p}_{ts} would occur even in the absence of jets. The inferred soft-component power-law $\bar{p}'_{ts}(S_0)$ trend in Fig. 14 (right) is consistent for all values of S_0 . Figure 15 (right) shows that if S_0 bias of \bar{p}_{ts} is corrected there is significant bias of $\bar{p}_{th}(n_s, S_0)$ beyond what is evident in Figs. 1 and 2 (b,d), but the bias magnitude is small compared to variation of jet production with n_{ch} .

(f) Just as for p_t spectra, the TCM provides a basic reference for understanding ensemble-mean \bar{p}_t trends. The TCM is not fitted to individual data sets or collision systems. It is, in effect, a global representation of a large data volume including yields, spectra and two-particle correlations from multiple A-B collision systems over a broad range of collision energies. Deviations of properly-corrected particle data from the TCM then reveal *differential details of the information carried by those data*.

These conclusions can be compared with those reported in Ref. [3]. In the introduction appears “The aim of this study is to investigate the importance of jets in high-multiplicity pp collisions and their contribution to charged-particle production at low p_T .” The contribution of jets to hadron spectra at lower p_t in p - p collisions has been established in a series of papers over fifteen years [10–13, 15, 28, 29], none of which is cited in Ref. [3]. The Ref. [3] abstract states “Within uncertainties, the functional form of $\langle p_t \rangle(n_{ch})$ is not affected by the sphericity selection,” but that statement conflicts with actual data properties as revealed in Fig. 15 (right). S_0 bias relating to the jet contribution to spectra is small compared to that for soft component \bar{p}_{ts} . Imposition of an S_0 condition on spectra does result in systematic bias of the jet-related spectrum hard component which is detected only by means of a highly differential analysis technique based on the TCM. As spectra and ensemble \bar{p}_t data are presented in Ref. [3] that information is inaccessible.

VII. SYSTEMATIC UNCERTAINTIES

Estimation of data systematic uncertainties typically addresses the reliability of numerical values resulting from physical measurements. In addition to inevitable statistical fluctuations the reliability of instrument calibrations and resulting data corrections is estimated. That approach is adequate if the interpretation of numerical values is unambiguous. In the present case where data volumes of 60M or 105M events are the basis for analysis systematic errors may dwarf statistical errors, making their correct estimation all that more important.

In this analysis the two-component model, a formal procedure with elements inferred from lower-energy p - p spectrum data, is used to separate two disjoint contributions to measured 13 TeV p - p p_t spectra. For the analysis of systematic uncertainties in this study both the accuracy of the separation and physical interpretation of the results are in question. This section addresses the following questions: (a) What is the overall accuracy of the TCM for p - p p_t spectrum data descriptions? (b) What is the significance and physical interpretation of selection-bias trends relative to the TCM? (c) What is the accuracy and interpretation of spectrum parametrizations related to jets? (d) What is the effect of sphericity as a basis for jet preference and the physical interpretation of results?

A. Overall accuracy of the TCM per Sec. III

Based on Figs. 6 and 8 it might be argued that the TCM shows highly significant deviations from p - p spectrum data and is therefore a poor model. But the TCM is a *predictive reference* based on a broad survey of yield, spectrum and correlation data [10, 11, 13, 14, 16, 17, 28] suggesting that the concept of systematic uncertainty should be reconsidered. How should the TCM be required to describe data and how well does it do that? Do significant data-model deviations reveal a faulty model or unexpected information carried by particle data?

In the present study the TCM is applied as a fixed reference to a minimum-bias ensemble of p - p p_t spectra sorted into multiplicity classes via two methods. The fixed TCM then provides highly differential information on resulting spectrum bias. If the TCM were fitted to individual spectra the bias trends would then be represented by varying fit parameters whose physical interpretation might be difficult. By examining resulting data deviations from a fixed model in relation to statistical errors as in Fig. 8 a likely physical interpretation may be possible that was not intuitively obvious beforehand.

The fixed TCM thus provides a valuable reference that is highly constrained by the requirement to describe p - p p_t spectra for all energies from 17 GeV to 13 TeV via simple systematic variation of model parameters and agreement with predictions based on jet data as illustrated in App. A. The model parameters that appear in Table I are those appearing in Table II with the following

exceptions: The values for q used in the present study are 4.0 and 3.8 respectively for 5 and 13 TeV whereas the values in Table II are 3.85 and 3.65. The values for σ_{y_t} used in the present study are 0.58 and 0.60 respectively for 5 and 13 TeV whereas the values in Table II are 0.58 and 0.615. Those changes arise because the 13 TeV spectrum data employed in Ref. [17] were in effect SPD data. In the present study it was decided to favor V0M data with the TCM. The motivation is evident in Fig. 9 (right). The values for α estimated in the present study are 0.0145 and 0.0170 whereas the values in Table II are 0.013 and 0.015 based on the earlier 13 TeV data with its limited n_{ch} reach (maximum $\bar{\rho}_0 \approx 12$ vs 54 for SPD in the later study) and 1M total events vs 60M for the later study. With those changes the TCM provides a good description of V0M data for the six highest n_{ch} classes as demonstrated in Fig. 8. Deviations for lower n_{ch} classes carry important new information about biases as noted.

The TCM may be further parametrized to describe n_{ch} trends of spectrum data in detail as illustrated in App. A. The n_{ch} dependence of 13 TeV SPD spectra can then be described within data uncertainties mainly by accommodating hard-component trends. The soft component exhibits no significant n_{ch} dependence in its shape. Within the TCM context variation of hard-component parameters with n_{ch} may then be physically interpreted in terms of mean jet characteristics altered due to selection bias.

B. Bias trends and “fit” quality per Sec. IV

For the Ref. [3] analysis three issues are important for data interpretation: (a) spectrum normalization for each n_{ch} class, (b) the jet contribution to spectra for each n_{ch} class and (c) selection bias for each n_{ch} class and each event selection method. Without a well-defined reference model it is difficult to distinguish among those issues.

Figure 16 (left) shows Fig. 10 (right) repeated for further consideration. The dashed curves for V0M/TCM and SPD/TCM spectrum ratios are those in Fig. 2 (b) and (d) for event classes II (V0M) and VII (SPD), each with $\bar{\rho}_0 \approx 20$. The data spectrum ratio SPD/V0M (solid) is consistent with the lower panel of Fig. 4 in Ref. [3]. The statistical noise artifact common to V0M and SPD spectra (dashed curves) cancels in ratio as an example of common-mode noise rejection. As noted in Sec. VB the SPD/V0M trend is interpreted by Ref. [3] to indicate that the V0M spectrum is “harder” than the SPD spectrum. However, comparison of the corresponding TCM reference spectra (dash-dotted) indicates that most of the deviation from unity is simply due to the difference in charge density $\bar{\rho}_0$ for the two event classes.

The data-model comparisons of Fig. 8 illustrate the statistical significance of the data-model deviations. It is useful to compare the “fit” quality of the TCM compared to V0M and SPD data spectra, although the TCM is not fitted to individual spectra. The quality of the data description for a given model can be estimated by the

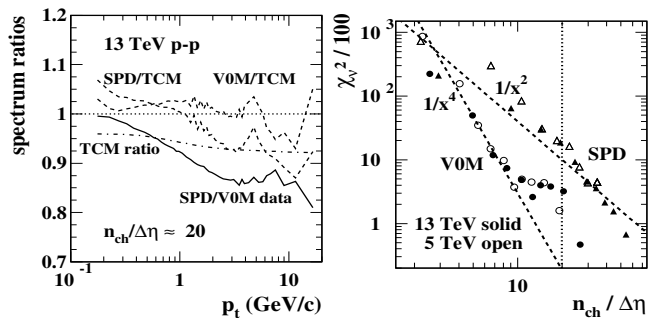


FIG. 16: Left: Repeat of Fig. 10 (right) for further discussion. Right: χ^2_ν values [second line of Eq. (15)] for each curve in Fig. 8. Data are observed to approximate power-law trends.

reduced χ^2 statistic χ^2_ν

$$\chi^2_\nu = \frac{1}{\nu} \sum_{i=1}^N \frac{(O_i - E_i)^2}{\sigma_i^2} \quad (15)$$

$$\approx \frac{1}{N} \sum_{i=1}^N Z_i^2,$$

where O_i are observations, E_i are model predictions and ν is the number of degrees of freedom – the number of observations N less the number of model parameters. In the present context a comparable model quality measure is approximated by the second line based on Z -scores as defined in Eq. (6). Since the TCM is not fitted to individual spectra and the resulting statistic is not compared to a χ^2 probability distribution the second form is applied.

Figure 16 (right) shows χ^2_ν values [second line of Eq. (15)] for each curve in Fig. 8. Note that χ^2 is ordinarily employed as a measure of goodness of fit but in the present case is a measure of the amount of *new information* carried by data relative to the TCM reference. The V0M and SPD trends are separately equivalent when comparing 5 TeV and 13 TeV data. Both event selection types happen to approximate power-law trends on \bar{p}_0 .

The vertical dotted line at $\bar{p}_0 = 20$ locates class II of V0M (20.5) and class VII of SPD (19.5) events for 13 TeV. There is a factor 5 difference between χ^2_ν values. However, the difference would be much greater if not for the structures in Fig. 16 (left) that are common to all spectra as noted in connection with Fig. 9 (left). Without that noise the higher n_{ch} classes of V0M events are approximately statistically consistent with the TCM.

C. Power-law fits: data vs TCM per Sec. V

This refers to Fig. 5 of Ref. [3] vs Fig. 9 of the present study and the substantial differences in the two results. One result arises from a power-law fit to a limited p_t interval; the other result is obtained with a log-derivative applied to spectrum data over a larger interval. The latter data are averaged over an interval chosen based on

differential data in Fig. 9 (left) that directly indicates what p_t interval can be approximated by a power law.

Numerically, the power-law model fits result in variation for V0M from 6.0 down to 5.7 and for SPD from 6.2 down to 4.9 whereas the log-derivative produces a fixed value 5.6 for V0M and variation from 5.7 down to 5.2 for SPD. The fixed log-derivative results for V0M are consistent with data/TCM ratios in Fig. 2 (d): i.e. no significant deviation from the TCM hard-component *shape* above $y_t = 4$. The same conclusion can be inferred from Fig. 4 (b). The varying n results for SPD are consistent with Eq. (A2) for $2/q$ in App. A. Note that plotting estimates of $2/q$ rather than q leads to a simple linear trend as in Fig. 17 (left) indicating that the effective high- p_t “width” of the spectrum hard component (i.e. $2/q$) increases linearly with SPD yield, an informative result.

It is unfortunate that relatively large artifacts appear in the data as sources of systematic uncertainty, as in Fig. 9 (left). The statistical power of 60 million 13 TeV events is thereby degraded, and in the case of the log-derivative requires rejecting the lowest and highest n_{ch} classes. Nevertheless, the consistency of both V0M and SPD exponent data with their respective smooth trends is indicative of the power of the log-derivative method.

D. Ensemble \bar{p}_t per Sec. VI

Although Ref. [3] estimates systematic uncertainties for ensemble \bar{p}_t (quoted as 1-2%) the substantial bias from incomplete p_t acceptance is not discussed. It is stated that “The efficiency correction [to \bar{p}_t]...is found to be $\sim 1\%$ ”, and “The effect of track cuts on $\langle p_T \rangle$ was found to be...of the order of 1%.” The only mention of the low- p_t cutoff is “This [primary particle composition] uncertainty takes into account the extrapolation of the spectra to low p_T ...” It is further stated that “The transverse momentum spectra...are *fully corrected*...[emphasis added].” As demonstrated in Sec. VIC the p_t cutoff bias to \bar{p}'_{ts} is about 0.1 GeV/c corresponding to 10-20% of the \bar{p}_t data values, compared to ALICE estimated systematic uncertainties $O(1\%)$ as noted above.

Given that the total excursion of uncorrected \bar{p}'_t in Fig. 13 (left) is about 65% of the soft-component value 0.48 GeV/c, *interpretation* of uncorrected data is problematic. The nominal goal of the ALICE spectrum study is determination of jet contributions to spectra, and \bar{p}_t data are essential for achieving that goal. But one can contrast Fig. 13 (left), where interpretation of the data is quite uncertain, with Fig. 13 (right) where separation of jet and non-jet contributions is accurately achieved.

Another important uncertainty relating to \bar{p}_t data interpretation is the consequence of event selection based on sphericity S_0 . It is expected that low sphericity will prefer “jetty” events and high sphericity will prefer “isotropic” events. The structure of Fig. 13 (left) obscures how the \bar{p}_t vs n_{ch} trend relates to jets whereas the corrected structure of Fig. 13 (right) brings clarity.

Given that clarification the simplicity of Fig. 15 (left) leads to the correct interpretation of “...within uncertainties the overall shape of the $[\bar{p}_t \text{ vs } n_{ch}]$ correlation...is not sphericity-dependent.” The correct interpretation is that while jet production varies approximately quadratically with n_{ch} , and jet production for SPD events increases ≈ 30 -fold relative to NSD p - p , sphericity has almost no effect on the jet contribution to spectra,

VIII. DISCUSSION

In its introduction Ref. [3] asserts that a p_t spectrum “carries information of the dynamics of soft and hard interactions.” As noted “The aim of [Ref. [3]] is to investigate the importance of jets in high-multiplicity pp collisions and their contribution to charged-particle production at low p_T .” It is proposed to “disentangle the energy and multiplicity dependence” of p_t spectra.” The TCM has been applied to p - p p_t spectra over three orders of magnitude of p - p collision energy, and after fifteen years of development arguably extracts all available information from p_t spectra [10, 16, 17]. The energy and multiplicity dependences of p_t spectra are indeed factorizable, but the energy dependence requires a large energy interval to identify systematic variations accurately; the interval 5 to 13 TeV is too small to do so [13, 17]. Given those observations it is instructive to consider certain comments within Ref. [3] relative to TCM results.

A. Spectrum evolution with n_{ch}

This topic mainly concerns Figs. 2 and 3 of Ref. [3] which present ratios of spectra for different n_{ch} classes, two energies and two event selection criteria to minimum-bias INEL > 0 spectra. It is noted that “the features of the spectra...are qualitatively the same for both energies” and only the 13 TeV result is further discussed. That strategy can be compared with “disentangle the energy and multiplicity dependence.” If two things are “qualitatively the same” then they are quantitatively *dissimilar*, i.e. the difference is information carried by p_t spectra.

Commenting on Figs. 2 and 3 “The [spectrum] ratios to the INEL > 0 p_T distribution exhibit two distinct behavior [sic].” In brief, at lower p_t the spectrum ratios exhibit small p_t dependence, but above 0.5 GeV/c the ratios are strongly dependent on n_{ch} and p_t . Referring to Fig. 2 is the comment “...the p_T spectra become harder as the multiplicity increases, which contributes to the increase of the average transverse momentum with multiplicity.” But the seemingly dramatic spectrum “hardening” in Fig. 2 does not dominate $\bar{p}_t(n_{ch})$ trends where the central issue is dijet production as a function of n_{ch} described comprehensively via the TCM [26, 27]. The term “hardening” is ambiguous between increased jet number with n_{ch} and possible bias of jet fragment distributions [11].

In abstract and main text is the statement “The high- p_T (> 4 GeV/c) yields of charged particles increase faster than the charged-particle multiplicity, while the increase is smaller [i.e. less rapid than n_{ch}] when we consider lower- p_T particles.” In relation to its Fig. 6 describing charge integrals within specific Δp_t intervals Ref. [3] observes “Despite the large uncertainties, it is clear the data show a non-linear [i.e. faster than n_{ch}] increase.” But the TCM has provided an accurate *quantitative* picture of such trends for fifteen years as noted above. The low- p_t part of spectra (< 0.5 GeV/c or $y_t \approx 2$) increases $\propto \bar{\rho}_s \approx \bar{\rho}_0 - \alpha \bar{\rho}_s^2$, i.e. slower than $\bar{\rho}_0 = n_{ch}/\Delta\eta$, whereas the higher- p_t part of spectra (i.e. > 4 GeV/c or $y_t \approx 4$) increases *precisely* $\propto \bar{\rho}_s^2$, i.e. approximately *quadratically* with n_{ch} . Again as noted, a characteristic aspect of certain observations in Ref. [3] is confusion among several issues: (a) spectrum normalization (or not), (b) jet production vs n_{ch} , and (c) various selection-bias effects.

B. Manifestations of jets in p_t spectra

Given a primary goal of Ref. [3] – determination of the jet contribution to particle production at lower p_t – it is difficult to find any responding result in the paper. Regarding spectra in relation to pQCD “...the high- p_T ($p_T > 10$ GeV/c) particle production is quantitatively well described by perturbative QCD (pQCD) calculations...” But no experimental evidence is presented relating jet contributions at higher p_t , or jet production in general, to hadron production at lower p_t . In contrast, the TCM quantitatively isolates minimum-bias jet contributions to hadron production over the entire p_t acceptance as in Sec. III C, and spectrum hard components have been quantitatively related to pQCD via *measured* jet energy spectra and fragmentation functions [11, 13].

Reference [3] does acknowledge information derived from model fits to spectra: “Commonly, the particle production is characterized by quantities like integrated yields or any fit parameter of the curve extracted from fits to the data, for example, the so-called inverse slope parameter $[T]$...” and then emphasizes power-law exponent n as relating to jet production. For description of spectra at higher p_t “the natural choice is fitting a power-law function...to the invariant yield [p_t spectrum?] and studying the multiplicity dependence of the exponent (n) extracted from the fit.” One conclusion – “the results [the $n(n_{ch})$ trend] using the two multiplicity estimators [V0M and SPD] are consistent within the overlapping multiplicity interval” – is problematic as argued below.

A mechanism for n_{ch} dependence of exponent n is conjectured as follows: “In PYTHIA 8, it has been shown that the number of high- p_T jets increases with event multiplicity.” In fact, the exact multiplicity dependence of jet production in inelastic p - p collisions is reported in Ref. [13] based on event-wise-reconstructed jet *measurements*, not a Monte Carlo. The conjecture continues: “...based on PYTHIA 8 studies, the reduction of the

power-law exponent $[n]$ with increasing multiplicity $[n_{ch}]$ can be attributed to an increasing number of high- p_T jets.” But for VOM event selection in Fig. 9 (right) the exponent n trend on n_{ch} is consistent with a *constant* (13 TeV) or even slight *increase* (5 TeV). The same jet population is accessible to either selection criterion and jet *number* is strictly dependent on n_{ch} as demonstrated by Fig. 12. All that differs is the spectrum bias at high p_t induced by the selection method. Such arguments confuse basic QCD jet production (with its well-established systematics) and manifestations of event selection bias.

The dijet production rate for NSD p - p collisions can be predicted from measured jet cross sections, and such predictions can be compared quantitatively with jet contributions to spectra and two-particle correlations identified by their unique n_{ch} dependence (e.g. as represented by the TCM) [11]. For 200 GeV NSD collisions 3% of events include a dijet per unit of eta [10]. For ≈ 10 TeV NSD collisions 15% of events include a dijet per unit of eta [13], where the quoted percentages are $100(1/\sigma_{\text{NSD}})d\sigma_{\text{jett}}/d\eta$. For a typical range of p - p charge densities $\bar{\rho}_0 \in [\bar{\rho}_{\text{NSD}}, 10\bar{\rho}_{\text{NSD}}]$ the dijet yield should increase by factor 100 due to the *observed* trend $\bar{\rho}_h \propto \bar{\rho}_s^2$. 13 TeV p - p collisions with SPD $\bar{\rho}_0 \approx 54$ should include 11 dijets per unit pseudorapidity on average. “Jets” here assumes a minimum-bias jet spectrum wherein most jets appear near 3 GeV (the effective jet spectrum mode).

C. Selection biases and QCD

The same minimum-bias INEL > 0 event ensemble is partitioned into ten multiplicity classes according to two selection criteria – VOM and SPD. The VOM or “forward [on η] multiplicity estimator” is said to “minimize the possible autocorrelations induced by the use of the midpseudorapidity estimator.” The statement suggests that the VOM criterion should produce substantially less bias. “The comparison of results obtained with these [VOM and SPD] estimators allows to understand potential biases from measuring the multiplicity and p_T distributions in overlapping η regions.” As with statements about jet contributions to lower p_t it is difficult to find within Ref. [3] any such understanding. In fact “bias” as in that sentence does not appear again in the paper.

For spectrum data plotted as ratios, as in Figs. 1 and 2 (b,d), selection bias from VOM and SPD criteria appear quite different. However, the apparent large high- p_t bias for SPD involves a tiny fraction of all particles and even a small fraction of jet fragments. When the two criteria are compared based on significance as in Fig. 8 the SPD high- p_t bias does not dominate the structure. Ironically, VOM bias is *at least as* significant as SPD bias and the p_t dependence is similar, contradicting the expectation that “autocorrelations” are minimized by disjoint η intervals.

Particle production and QCD dynamics must be strongly correlated between VOM and SPD acceptances. Hadron production at midrapidity depends in part on

a parton splitting cascade within each projectile proton that also contributes hadrons at larger η . Thus, fluctuations in VOM must be strongly correlated with fluctuations in SPD, albeit SPD has additional contributions from parton scattering and fragmentation to jets. Figure 8 reveals that fluctuations *correlated* between VOM and SPD are statistically dominant, whereas fluctuations in low-energy jet formation play a less-significant role.

D. Ensemble \bar{p}_t vs sphericity

As part of a strategy to identify jet contributions at lower p_t Ref. [3] introduces sphericity S_0 (effectively an azimuthal asymmetry measure): “The present paper reports a novel multi-differential analysis aimed at understanding charged-particle production associated to partonic scatterings with large momentum transfer and their possible correlations with soft particle production.” But most of the jet-related hard component arises from lower-energy partons [11, 13], and most fragments from any jet appear at low p_t [29]. “Transverse sphericity...has been proven to be a valuable tool to discriminate between jet-like and isotropic events...” That statement is based on material presented in Ref. [30] which is a study of various event-shape measures applied to PYTHIA simulations. It is not clear from that study what sphericity contributes to understanding real p - p collisions.

“Studying observables as a function of sphericity reveals interesting features.” Relative to the \bar{p}_t vs n_{ch} trend for the INEL > 0 ensemble average as a reference the trend for “isotropic” events (high S_0) “stays systematically below” the reference, whereas “...for jet-like events” (low S_0) the \bar{p}_t trend is consistently higher. The following observation is interesting: “Moreover,...the overall shape of the correlation $[\bar{p}_t(n_{ch})]$, i.e. a steep linear rise below $dN_{ch}/d\eta = 10$ followed by a less steep but still linear rise above, is *not sphericity-dependent* [emphasis added].”

That qualitative description relates to a confusing data trend arising from questionable analysis variables. The data trend for uncorrected $\bar{p}'_t(n_{ch})$ includes the misleading dependence expressed by Eq. (12) and hard-component suppression at lower n_{ch} exhibited in Fig. 8. In contrast, the approximate linear rise of corrected \bar{p}_t vs $\bar{\rho}_s$ in Fig. 13 (right) and Fig. 15 (left) is equivalent to the linear rise of integrated yields with $\bar{\rho}_s$ in Fig. 12. In other words, the TCM structure of Eq. (13) is equivalent to the TCM structure of Eq. (10). Jets control the *slope* of the linear trend over a large n_{ch} interval: in the absence of jets there would be no linear rise, i.e. the slope of the trend is a measure of jet production. By observing that \bar{p}_t vs n_{ch} trends in Fig. 13 (left), equivalent to trends in Fig. 15 (left), are “not sphericity-dependent” Ref. [3] admits that S_0 does little to control jet production in p - p collisions. That the high- S_0 and low- S_0 trends appear respectively systematically below and above the reference in Fig. 7 of Ref. [3] is a consequence of S_0 biasing the nonjet spectrum *soft* component as noted in Sec. VI C.

IX. SUMMARY

This article reports a study of high-statistics p_t spectra from 5 TeV and 13 TeV p - p collisions at the large hadron collider. This study is based on the two-component (soft + hard) model (TCM) of hadron production near midrapidity. The spectrum data and additional spectrum analysis were reported by the ALICE collaboration with the nominal goal to estimate jet contributions to p_t spectra, especially at lower p_t . Part of the motivation was a response to recent claims of “collective” behavior (flows) in small (asymmetric?) collision systems. The principal data presentation was p_t spectra for various event classes in ratio to an ensemble average over all collision events.

The TCM has been demonstrated over a number of years to be a valuable tool for isolating distinct hadron production mechanisms in A-B collisions. In particular, hadron contributions to spectra from jet-related production (hard component) are accurately distinguished (at the percent level) from nonjet production (soft component). The signature element of the TCM for p - p collisions is a *quadratic relation* between the hard component and soft component as inferred from spectrum data.

A major goal for the ALICE study was characterization of *selection bias* resulting from sorting collision events into classes according to particle yields in two different pseudorapidity η intervals denoted by SPD (midrapidity) and V0M (forward rapidity). If event classes are simply compared to an ensemble average the present study finds that three issues are consequently confused: (a) spectrum normalization, (b) the jet contribution to p - p spectra as it varies *in known ways* with multiplicity n_{ch} and (c) the selection bias in question. This study demonstrates that ratios of data spectra to TCM spectra remove issues (a) and (b) and expose selection bias (c) to direct study.

One aspect of the present study is introduction of the *Z-score* statistical measure: Whereas spectrum *ratios* tend to visually exaggerate deviations at higher p_t and suppress those at lower p_t Z-scores provide a measure of the *statistical significance* of data-model deviations. Data-model deviations at high p_t that seem to dominate ratios are actually only modestly significant whereas deviations at lower p_t are much more significant and *quite similar* for V0M and SPD event classifications.

The present analysis reveals that selection bias has two main manifestations depending on the event selection criterion. The spectrum soft component appears unaffected by selection method. The V0M and SPD selection methods both bias the lower- p_t parts of the jet-related hard component (fragment distribution) similarly. For lower charge multiplicities n_{ch} the peaked hard component is shifted to lower p_t , resulting in spectrum suppression at higher p_t (above the peak mode) and enhancement at lower p_t (below the mode). However, the high- p_t tails of spectra are negligibly affected by V0M selection but strongly affected by SPD selection: with increasing n_{ch} SPD spectrum tails become increasingly harder (smaller

power-law exponent). The combined effects suggest that selection bias responds to fluctuations in jet production in different ways depending on the relevant η acceptance.

Ensemble-mean \bar{p}_t data as a function of n_{ch} were obtained for different values of *sphericity* S_0 , a measure of the azimuth asymmetry of the vector $\vec{p}_t(\phi)$ distribution. The intent was to bias events according to their “jettiness,” a lower S_0 value expected to prefer events with more or more-frequent jets. The published \bar{p}_t data are biased because of the incomplete detector p_t acceptance (lower limit at 0.15 GeV/c) making data interpretation more difficult. In the present analysis the \bar{p}_t data are corrected and transformed to a TCM configuration with fixed soft-component contribution and hard component varying with n_{ch} in a manner that should reveal the jet contribution to \bar{p}_t . This study concludes that the main affect of S_0 selection on \bar{p}_t vs n_{ch} trends is bias of the \bar{p}_{ts} *soft* component. The effect on the hard component (i.e. jet contribution) is barely detectable. Given S_0 as an azimuth asymmetry measure, its lower values tend to suppress events where the soft component includes more high- p_t particles, thus reducing its ensemble-mean \bar{p}_{ts} .

In summary, the TCM is observed to be a necessary and sufficient description of p - p p_t spectra and arguably represents all information carried by spectrum data for unidentified hadrons. The TCM hard component has been quantitatively related to the properties of event-wise reconstructed jets. Determination of an accurate TCM for isolated spectra (rather than ratios) over a broad range of event multiplicities and event selection criteria as in the present study establishes an accurate and efficient representation of a large volume of spectrum data. The contribution of jets to p - p p_t spectra is accurately determined at the percent level and the consequences of several forms of event selection are isolated.

Appendix A: Previous 13 TeV data TCM

A previous TCM analysis of 13 TeV p - p spectra was reported in Ref. [17]. That study emphasized multiplicity and energy dependence of the spectrum hard component in the context of QCD theory and jet measurements. The 13 TeV p - p spectrum data as reported in Ref. [18] were quite limited as to range of event multiplicity – see the 13 TeV solid triangles and open circles in Fig. 17 (left) – and the presentation format was based on ratios of spectra from three n_{ch} classes to a minimum-bias INEL > 0 reference. It was required therefore to develop new techniques to isolate the hard and soft components for the three n_{ch} classes based on analysis of 200 GeV spectrum data for which the TCM structure is well-established [10]. In this appendix relevant results from Ref. [17] are reviewed to provide context for the present study of a much more extensive sample of 13 TeV p - p spectrum data.

1. Spectrum TCM multiplicity dependence

In Sec. III TCM model functions are held fixed for all n_{ch} classes and for both VOM and SPD. Systematic data biases are then revealed in a precise way. However, in Ref. [17] the TCM hard component was parametrized to accommodate the n_{ch} dependence of the hard-component shape for 13 TeV SPD spectra. In this subsection those results (for 200 GeV as well as 13 TeV) are reviewed and the quality of the data description is evaluated. The 200 GeV data are equivalent to Ref. [3] SPD with $|\eta| < 1.0$

Figure 17 (left) shows variation of two 200 GeV $\hat{H}_0(y_t)$ parameters with $\bar{\rho}_s$ (lower solid and dashed curves) that provides accurate description of spectrum ratios above the hard-component mode for all multiplicity classes. Optimized TCM parameters follow simple $\bar{\rho}_s$ trends

$$\begin{aligned} 2/q &= 0.373 + 0.0137(\bar{\rho}_s/\bar{\rho}_{s,ref}) \quad (\text{lower solid}) \quad (\text{A1}) \\ \sigma_{y_t} &= 0.385 + 0.09 \tanh(\bar{\rho}_s/4) \quad (\text{lower dashed}). \end{aligned}$$

The nominal parameter values for the 200 GeV *fixed* $\hat{H}_0(y_t)$ model are represented by the dotted and dash-dotted lines (corresponding to parameter values for $\bar{\rho}_s/\bar{\rho}_{s,ref} \approx 2$). Variation of two parameters in combination serves to broaden the hard-component model *above* the mode toward higher y_t . The saturation of σ_{y_t} at larger $\bar{\rho}_s$ is a consequence of increasing $2/q$. The transition on $\hat{H}_0(y_t)$ from Gaussian to exponential form then moves back toward the mode and the exponential/power-law tail increasingly dominates the higher- p_t structure. $\bar{\rho}_{s,ref}$ values are noted in the Fig. 17 caption.

The corresponding parameter trends for 13 TeV inferred from spectrum *ratios* in the earlier analysis of Ref. [17] are shown by the upper solid triangles and open circles. New values for $2/q$ (upper solid dots) are inferred in the present study via log derivative applied directly to 13 TeV SPD y_t spectra via Eq. (7) (upper line). Those results correspond accurately with n values plotted in Fig. 9 (right) obtained with Eq. (7) (lower line) demonstrating the correspondence $n \approx q + 1.8$. The $2/q$ data are well described by

$$2/q = 0.472 + 0.021(\bar{\rho}_s/\bar{\rho}_{s,ref}) \quad (\text{upper solid}). \quad (\text{A2})$$

Previous 13 TeV $2/q$ values derived from spectrum ratios in Ref. [17] (triangles) differ substantially from those in the present study and demonstrate the difficulty of deriving accurate results from limited spectrum ratios.

Figure 17 (right) shows variation of the 200 GeV hard-component width required to accommodate data *below* the mode in the form $1/\sigma_{y_t}^2$ (solid points). The solid curve through points is $13.5 \tanh[(\bar{\rho}_s - 3.1)/5]$. Also included is the trend for the width above the mode from the left panel and Eq. (A1) (lower) plotted as $1/\sigma_{y_t}^2$ (open points and dashed curve respectively) demonstrating correlation of the two trends. The two widths become equal near $\bar{\rho}_s \approx 5$, or $\bar{\rho}_s/\bar{\rho}_{s,ref} \approx 2$ in Fig. 17 (left) where the hard-component model is then, near its mode, approximately symmetric as in Refs. [10, 14].

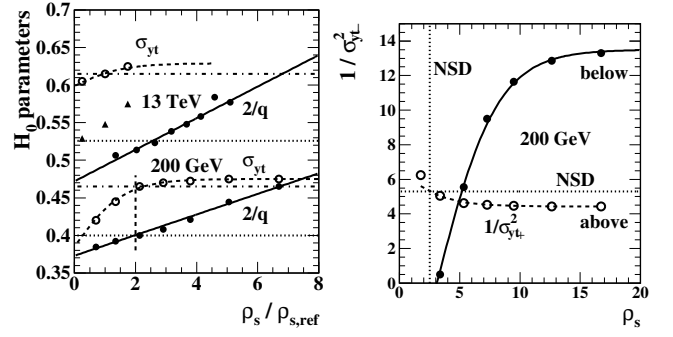


FIG. 17: Left: TCM hard-component parameters varying with n'_{ch} or $\bar{\rho}_s$ for a revised TCM. 200 GeV solid and dashed curves through parameter data are defined by Eqs. (A1). The 13 TeV open circles and solid triangles are as reported in Ref. [17]. The upper solid dots and solid line are updates determined in the present analysis, derived from more extensive p - p data. $\bar{\rho}_{s,ref} = 2.45$ for 200 GeV NSD p - p collisions and 5.8 for 13 TeV NSD collisions. The factor 2 in $2/q$ permits greater plot sensitivity. The mean-value energy trend for σ_{y_t} is shown in Fig. 20 (left) and for $1/q$ is shown in Fig. 19 (left). Right: Variation of the Gaussian width below the hard-component mode σ_{y_t-} (solid points) for $n = 2-7$ that accommodates data in that y_t interval. The Gaussian width above the mode σ_{y_t+} (open points) is included for comparison. The curves are defined in the text. The correlation of two trends is notable.

Figure 18 (left) summarizes the revised 200 GeV TCM hard-component model for six multiplicity classes. The hard component for the lowest p - p multiplicity class $n = 1$ is typically severely distorted due to selection bias (see Sec. III C for example).

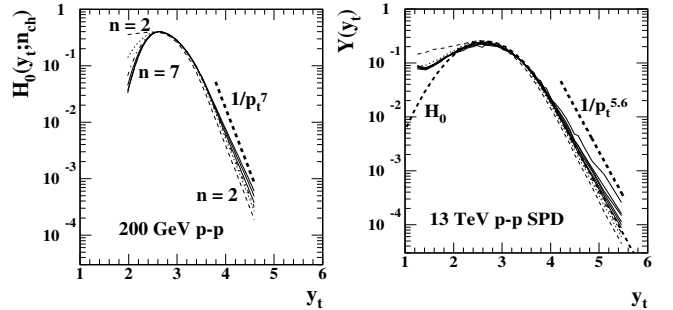


FIG. 18: Left: Evolution of the 200 GeV hard-component model over six multiplicity classes that exhausts all information in high-statistics spectrum data from Ref. [14]. Right: Spectrum hard components for SPD event selection and for nine multiplicity classes of 13 TeV p - p collisions. The order of line styles is reversed compared to other figures in this article to match the order in the left panel, and the order of index n is also reversed from the present study.

Figure 18 (right) shows 13 TeV SPD spectrum hard components (curves) appearing in Fig. 4 (d). SPD event selection based on particle yields within $|\eta| < 0.8$ is consistent with event selection for 200 GeV data based on yields within $|\eta| < 1$. Line types for this panel are reversed in order compared to other figures in this study

to match the convention in the left panel. As noted, the hard component for the lowest multiplicity class (here $n = 1$, not 10 as in the present study) is not shown since there is very little jet contribution to those events due to strong selection bias. Given those minor differences the event-selection biases for 200 GeV and 13 TeV p - p p_t spectra are remarkably similar. The similarity at higher p_t is consistent with the solid lines in Fig. 17 (left).

2. Spectrum TCM collision-energy dependence

Figure 19 (left) shows soft-component exponents in the form $1/n$ inferred from spectrum data for three collision energies (solid points) at the SPS, RHIC and LHC. The solid curve is an algebraic hypothesis based on variation of the soft component due to conjectured Gribov diffusion [31]. Low- x gluons result from a virtual parton splitting cascade within projectile nucleons whose mean depth on x is determined by the collision energy. Each step of the cascade adds transverse-momentum components in a random-walk process. The depth of the cascade is proportional to $\ln(s/s_0)$, and $\sqrt{s_0} \approx 10$ GeV is inferred from dijet systematics [13, 28]. Given the properties of a random walk and with $1/n$ as a measure of transverse-momentum excursions [32] its trend is estimated as $\propto \sqrt{\ln(\sqrt{s}/10 \text{ GeV})}$ (solid curve). The open circles at 0.9, 2.76 and 7 TeV are interpolations of the Lévy exponent to $n = 9.82$, 8.83 and 8.16 respectively.

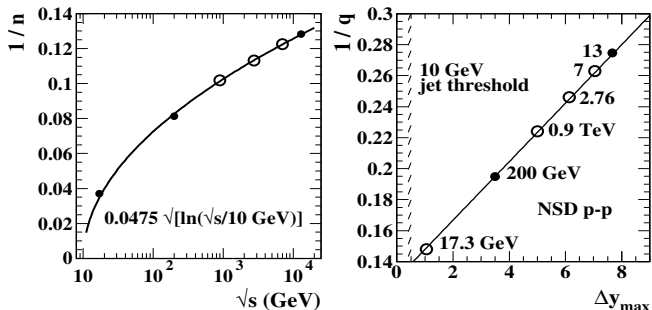


FIG. 19: Left: Measured Lévy exponents for three collision energies (solid points). The curve is a fit by eye of the function $A\sqrt{\ln(\sqrt{s}/10 \text{ GeV})}$ (with $A = 0.0475$) motivated by the possibility of Gribov diffusion controlling the growth of transverse momentum for low- x partons (gluons) [31]. Open symbols are interpolations at energies relevant to the study in Ref. [17]. Right: Hard-component exponents q determined by analysis of p - p spectrum data (solid points) from Ref. [14] and Ref. [17]. The solid curve is based on a jet-spectrum parametrization in Ref. [13] that also describes ensemble-mean- p_t hard-component energy variation [26]. Open points are interpolations and extrapolation relevant to Ref. [17].

Figure 19 (right) shows inverse values (solid points) of exponents $q = 5.15$ for 200 GeV and $q = 3.65$ for 13 TeV plotted vs quantity $\Delta y_{max} \equiv \ln(\sqrt{s}/6 \text{ GeV})$ that is observed to describe the energy trend for jet spectrum widths $\propto \Delta y_{max}$ from NSD p - p collisions assum-

ing a jet-spectrum low-energy cutoff near 3 GeV [13] (see Fig. 5 of Ref. [13] for a direct comparison with measured jet spectra). The inverse $1/q$ effectively measures the hard-component peak width at larger y_t . The relation $1/q \propto \Delta y_{max}$ (solid line) is expected given that the p - p p_t -spectrum hard component can be expressed as the convolution of a fixed p - p fragmentation-function ensemble with a collision-energy-dependent jet spectrum [11], and the jet-spectrum width trend has the same dependence [13]. The vertical hatched band indicates an inferred cutoff to dijet production from low- x gluon collisions near 10 GeV. That the same relation applies to the ensemble \bar{p}_t hard component was established in Ref. [26]. $1/q$ for $q = 3.80$ for 7 TeV, $q = 4.05$ for 2.76 TeV and $q = 4.45$ for 0.9 TeV (open circles) are interpolations.

Figure 20 (left) shows NSD TCM hard-component model parameters \bar{y}_t and σ_{y_t} (points) vs collision energy. The solid points are derived from data. The open points are interpolations or extrapolations derived from the inferred or predicted trends in the figure (curves). The trends for \bar{y}_t and σ_{y_t} are consistent with straight lines. Whereas σ_{y_t} increases by 50% the upper limit on \bar{y}_t variation is five percent (hatched band) and \bar{y}_t may not actually vary significantly over over three orders of magnitude of collision energy. The trend for \bar{y}_t is consistent with a fixed lower bound on the underlying jet spectrum near 3 GeV, also nearly independent of collision energy [11, 13].

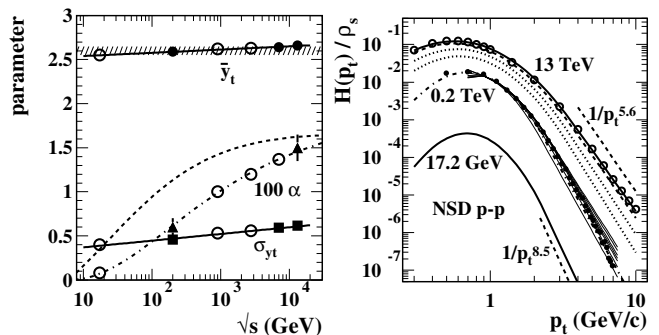


FIG. 20: Left: TCM NSD hard-component parameters derived from spectrum data (solid points). Open circles are interpolations or extrapolations relevant to Ref. [17]. The solid lines are fits to data. The dashed and dash-dotted curves related to $\alpha(\sqrt{s})$ are described in Ref. [17]. Right: Survey of spectrum hard components over the currently accessible energy range from threshold of dijet production (10 GeV) to LHC top energy (13 TeV). The curves are determined by parameters in Table II except for the 200 GeV fine solid curves determined also by the σ_{y_t} and q trends in Fig. 17 (left). The points are from Refs. [14] (200 GeV) and [18] (13 TeV).

Figure 20 (right) shows the TCM for quantity $H(p_t; E)/\bar{\rho}_s(E) \approx \alpha(E)\bar{\rho}_s(E)\hat{H}_0(p_t; E)$ measuring the spectrum hard component *per soft-component yield* corresponding to dijet production per participant low- x gluon. The two dotted curves are for 0.9 and 2.76 TeV and the dashed curve is for 7 TeV. Isolated hard components rather than spectrum ratios clarify spectrum en-

ergy evolution and its relation to dijet production. The hard-component mode on p_t is near 0.5 GeV/c ($y_t \approx 2$) whereas the mode on y_t is near 2.7 ($p_t \approx 1$ GeV/c).

The predictions for six collision energies (curves) derived from parameter values in Table II have been compared to data from four energies (13, 7, 0.9 and 0.2 TeV) [17]. The 17.2 GeV extrapolation indicates no *significant* jet contribution to yields and spectra at that energy and explains why no excess p_t fluctuations were observed at the SPS [33, 34]. However, evidence for SPS jets is visible in 17 GeV azimuth correlations as a more sensitive detection method [35]. The 200 GeV summary (thin solid) includes parametric variation of $\hat{H}_0(y_t; q, \sigma_{y_t}, n_s)$ for six multiplicity classes as described in Sec. A 1. Corresponding data (solid points) represent NSD p - p collisions. The overall result is a comprehensive and accurate description of dijet contributions to p_t spectra vs p - p collision energy over three orders of magnitude.

3. Spectrum TCM parameter summary

Table II summarizes NSD p - p TCM parameters for a broad range of energies. The entries are grouped as soft-component parameters (T, n), hard-component parameters ($\bar{y}_t, \sigma_{y_t}, q$), hard-soft relation parameter α and soft density $\bar{\rho}_s$. Slope parameter $T = 145$ MeV is held fixed

for all cases consistent with observations. Its value is determined solely by a low- y_t interval where the hard component is negligible. The interpolated Lévy exponent n values are derived from Fig. 19 (left) (open circles). Interpolated hard-component q values are derived from Fig. 19 (right) (open circles). $\bar{\rho}_s$ values are derived from the universal trend $\bar{\rho}_s \approx 0.81 \ln(\sqrt{s}/10 \text{ GeV})$ inferred from correlation and yield data. All 0.9 and 2.76 TeV values are predicted via interpolation. All remaining (unstarred) numbers are obtained from spectrum data.

TABLE II: Spectrum TCM parameters for NSD p - p collisions at several energies from Ref. [17]. Starred entries are estimates by interpolation or extrapolation. Unstarred entries are derived from yield, spectrum or spectrum-ratio data.

\sqrt{s} (TeV)	T(MeV)	n	\bar{y}_t	σ_{y_t}	q	100α	$\bar{\rho}_s$
0.0172	145	27	2.55*	0.40*	6.75*	0.07*	0.45
0.2	145	12.5	2.59	0.435	5.15	0.6	2.45
0.9	145	9.82*	2.62*	0.53*	4.45*	1.0*	3.65
2.76	145	8.83*	2.63*	0.56*	4.05*	1.2*	4.55
5.0	145	8.47*	2.63*	0.58*	3.85*	1.3*	5.00
7.0	145	8.16*	2.64	0.595	3.8*	1.4*	5.30
13.0	145	7.80	2.66	0.615	3.65	1.5	5.80

-
- [1] V. Khachatryan *et al.* (CMS Collaboration), JHEP **1009**, 091 (2010).
- [2] K. Dusling, W. Li and B. Schenke, Int. J. Mod. Phys. E **25**, no. 01, 1630002 (2016).
- [3] S. Acharya *et al.* (ALICE collaboration), Eur. Phys. J. C **79**, no.10, 857 (2019).
- [4] S. Acharya *et al.* (ALICE), Phys. Rev. C **99**, no.2, 024906 (2019).
- [5] V. Khachatryan *et al.* (CMS), Phys. Lett. B **765**, 193-220 (2017).
- [6] J. Adam *et al.* [ALICE], Nature Phys. **13**, 535-539 (2017).
- [7] M. Gyulassy and L. McLerran, Nucl. Phys. A **750**, 30 (2005).
- [8] E. Avsar, Y. Hatta, C. Flensburg, J. Y. Ollitrault and T. Ueda, J. Phys. G **38**, 124053 (2011).
- [9] K. Jiang *et al.*, Phys. Rev. C **91**, 024910 (2015).
- [10] J. Adams *et al.* (STAR Collaboration), Phys. Rev. D **74**, 032006 (2006).
- [11] T. A. Trainor, Phys. Rev. C **80**, 044901 (2009).
- [12] T. A. Trainor and D. T. Kettler, Phys. Rev. C **83**, 034903 (2011).
- [13] T. A. Trainor, Phys. Rev. D **89**, no.9, 094011 (2014).
- [14] T. A. Trainor and D. J. Prindle, Phys. Rev. D **93**, 014031 (2016).
- [15] T. A. Trainor, Int. J. Mod. Phys. E **17**, 1499 (2008).
- [16] T. A. Trainor, J. Phys. G **47**, no.4, 045104 (2020).
- [17] T. A. Trainor, J. Phys. G **44**, 075008 (2017).
- [18] J. Adam *et al.* (ALICE Collaboration), Phys. Lett. B **753**, 319 (2016).
- [19] B. B. Abelev *et al.* (ALICE Collaboration), Phys. Lett. B **728**, 25 (2014).
- [20] F. Antinori *et al.*, arXiv:1604.03310.
- [21] G. Pancheri and Y. Srivastava, Conf. Proc. C **850313**, 28 (1985) [Phys. Lett. B **159**, 69 (1985)].
- [22] Gubner, John A. (2006). *Probability and Random Processes for Electrical and Computer Engineers*, Cambridge University Press, p. 388.
- [23] C. Flensburg and G. Gustafson, JHEP **10**, 014 (2010).
- [24] E. Kreyszig (1979). *Advanced Engineering Mathematics* (Fourth ed.), Wiley, p. 880, Eq. 5.
- [25] B. B. Abelev *et al.* (ALICE Collaboration), Phys. Lett. B **727**, 371 (2013).
- [26] T. A. Trainor, Phys. Rev. C **90**, no. 2, 024909 (2014).
- [27] T. A. Trainor, arXiv:1708.09412.
- [28] G. Agakishiev, *et al.* (STAR Collaboration), Phys. Rev. C **86**, 064902 (2012).
- [29] T. A. Trainor and D. T. Kettler, Phys. Rev. D **74**, 034012 (2006).
- [30] A. Ortiz, Adv. Ser. Direct. High Energy Phys. **29**, 343-357 (2018).
- [31] Y. L. Dokshitzer and D. E. Kharzeev, Ann. Rev. Nucl. Part. Sci. **54**, 487 (2004).
- [32] G. Wilk and Z. Włodarczyk, Phys. Rev. Lett. **84**, 2770 (2000).
- [33] H. Appelshäuser *et al.* (NA49 Collaboration), Phys. Lett. B **459**, 679 (1999).
- [34] T. A. Trainor, Phys. Rev. C **92**, 024915 (2015).
- [35] G. Agakishiev *et al.* (CERES/NA45 Collaboration), Phys. Rev. Lett. **92**, 032301 (2004).